Incretin mimetics restore the ER-mitochondrial axis and switch neuronal fate towards survival

Theodora Panagaki[a,b,*], Elisa B. Randi[a], Csaba Szabo[a], Christian Hölscher[b,c,*]

[a] *Chair of Pharmacology, Faculty of Science & Medicine, University of Fribourg, Fribourg, 1700, Switzerland*
[b] *Division of Biomedical & Life Sciences, Faculty of Health & Medicine, Lancaster University, Lancaster, LA1 4YG, UK*
[c] *Research & Experimental Center, Henan University of Chinese Medicine, Zhengzhou, 450046, China*

Abstract

Background and Purpose: Amyotrophic lateral sclerosis with associated frontotemporal dementia, Alzheimer's disease, Huntington's disease, and Parkinson's disease are the major neurodegenerative disorders that afflict more than 7 million people worldwide. There are no disease-modifying or disease-retarding therapeutic agents currently available on the market. All four conditions feature several seemingly-disparate pathological and genetic lesions, which, however, converge into calcium dyshomeostasis and a disturbed function of the axis of the endoplasmic reticulum (ER) and mitochondria.

Experimental Approach: Incretin mimetics – traditionally anti-diabetic therapeutic agents – have been repeatedly shown to exert neurotrophic effects in neuroblastoma cells, rodent primary neurones, and murine models of neurodegeneration. Herein, for the very first time, we assess the pharmacological effects of Liraglutide and the dual incretin DA-CH3 in terminally differentiated human neurones under conditions of calcium-dependent chronic ER stress and additionally assess their efficacy in one of the most critical regulatory point for neurones, the mitochondrial respiration and dynamics.

Key Results: Liraglutide and DA-CH3 rescue the arrested oxidative phosphorylation and glycolysis. They mitigate the suppressed mitochondrial biogenesis and hyper-polarisation of the mitochondrial membrane, all, to re-establish normalcy of cellular bioenergetics under conditions of chronic ER stress. These effects correlate with a resolution of the unfolded protein response and the autophagic arrest to halt the excessive synaptic and neuronal death, with the dual incretin displaying a superior anti-apoptotic effect.

Conclusions: Our findings pave the way for a therapeutic strategy for disorders with a considerable social-economic burden and deepen our understanding of the spectrum of the incretin-signalling functions.

Keywords: Liraglutide, GLP-1/GIP dual agonist, ER stress, cellular bioenergetics, $\Delta\Psi_m$, mitochondrial biogenesis, autophagy, incretin signalling, neuroprotection

*Corresponding authors

Email addresses: theodora.panagaki@unifr.ch (Theodora Panagaki), christian_holscher@mac.com (Christian Hölscher)

URL: http://www.christian-holscher.info/index.html (Christian Hölscher)

1. Introduction

The neuropathological cascade begins years prior to the clinical onset of cognitive and brain-structural impairments in human disease. It alters the proteostasis network, calcium dynamics, and mitochondrial function gradually favouring the aberrant deposition of misfolded proteins and synapse degeneration. The buffering capacity and integrity of these processes lie in the homeostasis of the endoplasmic reticulum (ER) (Martínez et al., 2017, 2018). The ER is a dynamic membrane system that extends from the soma to the entire dendrite arbour, including some dendritic spines, and the axon of the neurone (Ramírez and Couve, 2011) that, in a dynamic cross-talk with most intercellular organelles via membrane contact sites, provides the major platform for autophagosome (Ktistakis, 2020; Senft and Ronai, 2015) and mitochondrial biogenesis (Friedman et al., 2011; Korobova et al., 2013). The ER is additionally the fundamental sub-cellular compartment for protein synthesis and quality control of approximately one-third of the total proteome, including all plasma membrane channels and receptors important for synaptic function (Martínez et al., 2018; Schroder and Kaufman, 2005). It also is the major calcium storage depot in the cell (Stutzmann and Mattson, 2011).

Calcium release from the ER mediates neurotransmitter exocytosis at the pre-synapse whilst potentiating gene transcription and modulating membrane excitability and dendritic spine structure for post-synaptic plasticity (Stutzmann and Mattson, 2011; Korkotian and Segal, 1998; Mellström and Naranjo, 2001). Upon release, the sarcoplasmic/ER calcium ATPase (SERCA) channel buffers calcium re-uptake from the cytosol into the ER to replenish the local calcium stores (Stutzmann and Mattson, 2011). A potential depletion of ER calcium stores will preclude the functionality of local molecular chaperones that closely monitor and assist folding, maturation and the delivery of secretory and membrane proteins. As such, the former results in a rise of the unfolded or misfolded protein load within the organelle lumen, a cellular state defined as ER stress (Schroder and Kaufman, 2005). In turn, the cell activates an adaptive signalling network, known as the unfolded protein response (UPR). The UPR engages the three ER-resident transmembrane stress transducers – the protein kinase RNA-like ER kinase (PERK), activating transcription factor 6 (ATF6) and inositol-requiring enzyme 1 (IRE1), which initially attenuate global protein synthesis, potentiate the transcription of chaperone proteins, and degrade the abnormal protein load through the proteasome (ER-associated degradation) and lysosome-mediated autophagy to safeguard proteostasis (Martínez et al., 2017; Schroder and Kaufman, 2005). ER stress further stimulates an early increase in mitochondrial respiration that depends crucially upon inter-organelle coupling and calcium transfer and establishes the bioenergetic sources required for the adaptation to this response (Bravo et al., 2011). However, upon stress chronicity, the UPR adapts its dynamics and shifts cell fate towards apoptosis through diverse but often overlapping mechanisms, including autophagy fail, bioenergetic crisis, the transcription of CAAT/enhancer-binding protein (C/EBP) homologous protein (CHOP), caspase activation, and aberrant expression and activity patterns of Bcl-2 family members along with their mediators (Martínez et al., 2017).

It is therefore intuitive that therapeutic interventions which mitigate the UPR towards a balance between protein generation and degradation and promote homeostasis along the ER/mitochondrial axis may benefit the clinical outcome of neurodegenerative disorders (Martínez et al., 2017, 2018). With this regard, the present study addresses the restorative effects of the glucagon-like peptide 1 (GLP-1) analogue, Liraglutide and the dual incretin analogue DA—CH3 in mitochondrial dynamics, autophagy, proteostasis signalling, synapse damage, and cytotoxicity under conditions of calcium-dependent, chronically-persistent ER stress in post-mitotic neurones from the human embryonic

neuronal precursor LUHMES cells. Liraglutide and DA-CH3 co-treatments rescue the arrested oxidative phosphorylation and glycolysis. They mitigate the suppressed mitochondrial biogenesis and hyper-polarisation of the mitochondrial membrane, all, to re-establish normalcy of cellular bioenergetics under conditions of chronic ER stress. These effects correlate with a resolution of the unfolded protein response and normalisation of the expression of 'core' autophagy components to ultimately halt the ectopic deficiency in major synaptic components and the excessive neuronal death, with the dual incretin displaying a stronger anti-apoptotic effect following persistent ER stress. Our study provides the first evidence for incretin-driven regulation of the aberrant ER/mitochondrial axis in human neurones, paving the way for a therapeutic strategy for disorders with a considerable social-economic burden.

2. Materials & Methods

2.1. Materials

Cell proliferation kit II [2,3-Bis-(2-methoxy-4-nitro-5-sulphophenyl)-2H-tetrazolium-5-carboxanilide (XTT)], and Cytotoxicity Detection Kit^{PLUS} [lactate dehydrogenase (LDH)] were purchased from Roche Diagnostics Ltd (West Sussex, UK). Agilent Seahorse XF Glycolytic Rate Assay (103344-100) and Cell Mito Stress Test (103015-100) kits, Seahorse XF24 cell culture microplates, and the corresponding Seahorse XF assay media and calibrant solution were acquired from Agilent Technologies AG (Basel-Stadt, Switzerland). Bovine serum albumin (BSA), tris buffered saline (TBS; pH 8.0) supplemented or not with 0.05% Tween® 20, phosphate buffered saline (PBS; pH 7.4), fibronectin from human plasma (0.1%), poly-L-ornithine solution ($MW = 30,000 - 70,000$; $0.1\,\mathrm{mg\,mL^{-1}}$), N^6 2'-O-Dibutyryl cAMP (adenosine-3',5'-cyclic monophosphate) sodium salt, tetracycline hydrochloride (BioReagent, suitable for cell culture), dimethyl sulphoxide (DMSO; anhydrous, $\geq 99.9\%$), and para-formaldehyde were obtained from Sigma-Aldrich Corporation (Dorset, UK). Human recombinant glial-derived neurotrophic factor (GDNF) was obtained from R&D Systems (Bio-Techne Ltd, Oxfordshire, UK). Quick Start™ Bradford protein assay kit was obtained from BIO-RAD Laboratories Ltd (Hertfordshire, UK). MitoBiogenesis™In-Cell ELISA Kit (Colorimetric; ab110217), JC-1 – Mitochondrial Membrane Potential Assay Kit (ab113850), and normal goat serum were purchased from Abcam (Cambridgeshire, UK). VECTASHIELD antifade mounting medium with DAPI were purchased from Vector Laboratories Ltd (Cambridgeshire, UK). Other materials and reagents for cell culture, Western blotting, and immunocytochemistry were obtained from Fisher Scientific UK Ltd (Leicestershire, UK), unless otherwise stated.

2.2. Cell culture

The Lund human mesencephalic (LUHMES) cell line is a sub-clone of the tetracycline-controlled, v-myc-over-expressing foetal human mesencephalic-derived cell line MESC2.10, established and characterised at Lund University (Lund, Sweden) (Lotharius et al., 2002, 2005). The LUHMES cell line (ATCC® CRL-2927™, RRID:CVCL_B056) was obtained from LGC Standards. Proliferating LUHMES cells were cultured in Advanced DMEM / F-12 supplemented with 1X Glutamax™, 1X N-2 supplement, and $40\,\mathrm{ng\,mL^{-1}}$ basic recombinant human fibroblast growth factor (bFGF) (hereinafter referred to as complete growth medium) in culture vessels, which were sequentially pre-coated with $50\,\mathrm{\mu g\,mL^{-1}}$ poly-L-ornithine and $1\,\mathrm{g\,mL^{-1}}$ fibronectin to promote cell attachment. Cells were maintained at 37 °C in a humidified incubator with 5% CO_2 and 95% air. Culture medium was renewed every 1 to 2 days.

2.2.1. Coating procedure for culture vessels

Nunc™ Cell Culture Treated EasY Flasks, Nunc™ MicroWell™ flat-bottomed 96-well plates, Seahorse XF24 cell culture microplates, and Millicell EZ SLIDE eight-well glass chamber slides were pre-coated overnight with 50 µg mL^{-1} poly-L-ornithine at room temperature. Following the removal of the poly-L-ornithine solution, the culture vessels were rinsed three times with Gibco® Water for Injection for Cell Culture and allowed to air-dry uncapped in a biological safety cabinet. Subsequently, the culture vessels were coated with 1 g mL^{-1} fibronectin for 3 h at 37 °C. Fibronectin solution was then removed, and all the vessels were rinsed three times with Gibco® Water for Injection for Cell Culture and allowed to air-dry uncapped in a biological safety cabinet. When dry, the culture vessels were filled with the appropriate culture medium and placed for at least 30 min in the incubator to allow the medium to reach its normal pH (7.0–7.6) and avoid excessive alkalinity of medium during cell handling procedures. Alternatively, they were sealed and stored under aseptic conditions in 4 °C for up to a week. Poly-L-ornithine and fibronectin were diluted at the required concentration in Gibco® Water for Injection for Cell Culture and Hank's balanced salt solution (HBSS), respectively, immediately before used.

2.2.2. Sub-culturing procedure

Proliferating LUHMES cells were sub-cultured when 70–80% confluent and grown up to passage 10 to avoid senescence and loss of pluripotency. Initially, the spent culture medium was discarded and the cell monolayer was gently rinsed with Dulbecco's phosphate-buffered saline (DPBS) that was formulated without calcium and magnesium. Subsequently, the cell monolayer was incubated with the TrypLE™ Select CTS™ dissociation reagent at 37 °C for $\sim$ 5 min. Cells were collected by centrifugation at 200 $\times$ g for 7 min and suspended in complete growth medium for the cell line. Viable cells were counted and seeded at the desired cell density for the differentiation procedure using the Countess™ Automated Cell Counter. Alternatively, proliferating LUHMES cells were seeded at 1 : 10 ratio.

2.2.3. Differentiation procedure

Differentiation procedure was conducted as previously described (Scholz et al., 2011). Briefly, 1×10^7 proliferating LUHMES cells were seeded into pre-coated T175 Nunc™ Cell Culture Treated EasY Flasks in the appropriate complete growth medium. Twenty-four hours post seeding, spent medium was discarded and replaced with the differentiation medium that defines day 0 (d 0) of the differentiation procedure. Differentiation medium consisted of Advanced DMEM/F12 medium supplemented with 1X Glutamax™, 1X N-2 supplement, 2 ng mL^{-1} human recombinant GDNF, 1 mM N^6 2'-O-Dibutyryl cAMP sodium salt, and 1 µg mL^{-1} tetracycline hydrochloride. At d 2, pre-differentiated LUHMES cells were sub-cultured at the density of 2×10^5 cells ml^{-1} into the corresponding culture vessels for each assay. Differentiation process continued for additional 3 to 4 days to allow cells to morphologically and biochemically mature into post-mitotic neurones. Differentiation medium was changed at d 4 of the differentiation procedure.

2.3. Cell treatments

All agents for cell treatment were handled as previously described (Panagaki et al., 2017). Briefly, thapsigargin reconstituted in 100% DMSO at a stock concentration of 1 mM, aliquoted and stored at −20 °C until used. For the experiments, thapsigargin stock preparations were serially diluted in differentiation medium at final working concentrations of 100 nM, containing 0.01% DMSO; DMSO concentration up to 0.33% has no impact on LUHMES cell viability and neurite

Name	Amino acid sequence	MW (Da)	Reference
Liraglutide	HAEGTFTSDVSSYLEGQAA[Lys-γE-C16 acyl]EFIAWLVRGRG–OH	3751.26	(Finan et al., 2013)
GLP-1/GIP dual agonist	YXEGTFTSDYSIYLDKQAAXEFVN WLLAGGPSSGAPPPS[Lys-C16]–NH_2	4234.63	(Finan et al., 2013)

Table 1: **Amino acid sequence and molecular weight (MW) of the incretin mimetics used in the current study**. Wherein the sequences, the "X" symbol stands for aminoisobutyric acid.

outgrowth (Stiegler et al., 2011).

The incretin mimetics were purchased from Chinapeptides Co., Ltd and Biochem Ltd (Shanghai, China). The purity of the peptides was analysed by reverse-phase high performance liquid chromatography (HPLC) and characterised using matrix-assisted laser desorption/ionisation time-of-flight (MALDI–TOF) mass spectrometry. The purity of the peptides tested was $\geq 96\%$ in accord with the manufacturers' reports. The amino acid sequences of the peptides tested herein are described in **Table 1**. The peptides were maintained in powdered, desiccated form at $-80\,^{\circ}\mathrm{C}$ and reconstituted in Gibco® Water for Injection for Cell Culture to to a concentration of $1\,\mathrm{mg\,ml^{-1}}$, aliquoted and stored at $-20\,^{\circ}\mathrm{C}$ until used. For the experiments, Liraglutide and GLP-1/GIP Dual Agonist stock preparations were diluted in differentiation medium to a final working concentration of 100 nM. The concentration was selected on the basis of previous experiments in which our group has established optimal working concentrations for the neuroprotective and anti-apoptotic effects of incretin mimetics (Panagaki et al., 2017).

All cell treatments were conducted at d 6 of the differentiation and at least in triplicate per assay per experiment.

2.4. Assessment of neuronal cell viability

Sixteen hours post-treatment initiation, we quantified neuronal cell viability with the Cell proliferation kit II (XTT) and Cytotoxicity Detection Kit$^{\mathrm{PLUS}}$ (LDH), as per our previously published methodology (Panagaki et al., 2017, 2020a,b).

2.5. Assessment of neuronal bioenergetics

Extracellular flux (XF) analysis was employed for the real-time quantification of mitochondrial respiration and glycolysis in live neurones. Specifically, we determined the oxygen consumption rate (OCR) owing to ATP turnover, proton leak and maximal respiratory capacity and the proton efflux rate (PER) from glycolytic and mitochondrial-derived acidification with the Agilent Seahorse XF Cell Mito Stress Test kit and Agilent Seahorse XF Glycolytic Rate Assay kit, respectively. Both assays were formatted into pre-coated Seahorse XF24 cell-culture microplates and performed as previously described (Panagaki et al., 2020a,b).

2.6. Assessment of mitochondrial membrane potential ($\Delta\Psi_m$)

We assessed $\Delta\Psi_{\mathrm{m}}$ with the 5,5',6,6'-Tetrachloro-1,1',3,3'-tetraethyl-benzimidazolylcarbocyanine iodide (JC-1); JC-1 is a lipophilic, cationic dye that naturally exists in monomers and fluoresces in the green spectrum. JC-1 typically enters and accumulates into the energised and negatively-charged mitochondria where it concentration-dependently forms reversible complexes (aggregates)

with a fluorescent emission and excitation at the red spectrum. However, under unhealthy conditions during which mitochondria feature an increased permeability and the loss of electrochemical potential, JC-1 does not reach the sufficient concentration for the formation of aggregates and thus retains its original green-fluorescent monomeric form. The ratio of the red-to-green fluorescence signal that reflects the ratio of the aggregated over the monomeric forms of JC-1 is an indicator of mitochondria polarisation (Perry et al., 2011).

The assay was formatted into into pre-coated Nunc™ MicroWell™ flat-bottomed black 96-well plates. Sixteen hours post-treatment initiation, neurones were washed once with pre-warmed 1X dilution buffer (kit provided) and incubated with 20 µM JC-1 for 10 min at 37 °C in a humidified incubator with 5% CO_2 and 95% air. Following JC-1 staining and two subsequent washes with pre-warmed 1X dilution buffer, microplates were read with Infinite® 200 PRO microplate reader at $\lambda_{\text{excitation}} = 535$ nm and $\lambda_{\text{emission}} = 590$ nm and at $\lambda_{\text{excitation}} = 475$ nm and $\lambda_{\text{emission}} = 530$ nm to monitor aggregated and monomer forms of the dye, respectively. Acquired fluorescent signal for each JC-1 form was initially normalised to the background and then used for calculating the ratio of aggregated to monomer JC-1. The latter was subsequently normalised to the corresponding (per condition) Janus Green cell normalisation stain. Janus green dye (ab111622) was obtained by Abcam (Cambridgeshire, UK) and the staining was performed in accord to the manufacturer's protocol.

2.7. Assessment of mitochondrial biogenesis

In-cell colourimetric ELISA assay was employed for quantitative measurement of the protein expression ratio of the cytochrome c oxidase subunit I (COX1; mitochondrial DNA-encoded protein) to the succinate dehydrogenase (SDHA; nuclear DNA-encoded protein) to monitor mitochondrial biogenesis. The assay was formatted into pre-coated Nunc™ MicroWell™ flat-bottomed transparent 96-well plates. Sixteen hours post-treatment initiation, neurones were fixed in 4% paraformaldehyde in 1X PBS for 10 min at room temperature and subsequently washed thrice with 1X PBS. Endogenous alkaline phosphatase activity was blocked with a 5 min-incubation with 0.5% acetic acid and neurones were then permeabilised in 1% Triton-X-100 in 1X PBS for 30 min at room temperature with gentle agitation. After a two-hour blocking step, neurones were probed with the provided primary antibody cocktail overnight at 4 °C with gentle agitation. The following day, neurones were briefly washed with PBS supplemented with 2% Tween®-20 and incubated with the provided AP/HRP-labelled secondary antibody solution for 1 h at room temperature with gentle agitation. AP and HRP development were respectively used for the kinetic detection of the protein levels of SDH-A and COX-1 at 405 and 600 nm over a cycle of 15 min with a inter-measurement interval time of $\sim$ 60 s.

2.8. Immunocytochemistry

Immunocytochemical experiments were formatted into pre-coated Millicell EZ SLIDE eight-well glass chamber slides. Sixteen hours post-treatment initiation, neurones were fixed, permeabilised and stained for Nrf2 in accord to the previously described protocol (Panagaki et al., 2017).

2.9. Protein extraction & Immunoassays

Sixteen hours post-treatment initiation, neurones were washed twice with ice-cold 1X PBS and harvested in 1X PathScan® Sandwich ELISA cell lysis buffer supplemented with protease/phosphatase

inhibitor cocktail (1X). After two freeze/thaw cycles, the whole-cell lysate was collected and sonicated for 1 min (5 s ON/5 s OFF – 6 cycles). The total protein was extracted by centrifugation at $\sim 16000 \times g$ at 4 °C for 15 min. The Quick start™ Bradford protein assay was conducted to estimate the protein concentration of the samples. Protein samples of whole-cell lysate were aliquoted and stored at −80 °C till processed for Western blotting and PathScan® Intracellular Signaling ELISA Array (#14471, Cell Signaling Technology, Greater London, UK). Both immunoassays were conducted in accord to our previously published methodology (Panagaki et al., 2017). The primary antibodies used in the Western blotting experiments are summarised in **Table S1**. The intercellular signalling targets of the array are listed in **Figure S1**.

2.10. Statistics

All the results were expressed as mean ± standard error (SEM) of five independent experiments. Assumption of normality was examined with D'Agostino-Pearson's K-squared and Shapiro-Wilk tests. Differences among means were considered significant if $p \leq 0.05$. Data processed with two-way ANOVA analysis, followed by *post-hoc* Bonferroni's multiple-comparison *t*-tests to identify differences among experimental groups and effects of incretin treatments under control and ER-stressed conditions. We employed repeated-measures three-way ANOVA, followed by *post-hoc* Bonferroni's multiple-comparison *t*-tests, to analyse the effects of each incretin in the mitochondrial biogenesis under control and ER-stressed conditions over time. Statistical calculations were performed in GraphPad Prism 8 (GraphPad Software Inc., San Diego, USA) for Mac OS X software.

2.11. Research Ethics Statement

No ethical approval was required for the present study. All experiments, image acquisition, and cell treatments were performed in a blinded fashion.

2.12. Data Availability Statement

All data supporting the findings of this study are included in this published article and its supplementary information file.

3. Results

3.1. The GLP-1/GIP dual agonist maximises the incretin-derived benefit on attenuating the neuronal UPR upon chronic ER stress.

We initially quantified the expression of transducers, mediators of the UPR by Western blotting, as shown in **Figure 1**. Chronic thapsigargin treatment potentiates a two-fold increase in the ER-stress sensor BiP and almost halves the protein levels of the full-length (90 kDa) UPR transducer – ATF6 that may signify its truncation and downstream activation (Panagaki et al., 2017; Wang et al., 2000). Chronic thapsigargin additionally precludes the engagement of Ire1α in the neuronal UPR, evident by the one-fold decrease in the expression of the phosphorylated at the serine 724 residue (Ser724) over the total protein levels, and disrupts the oxidative folding machinery within the ER lumen by diminishing the availability of the lectin chaperone calnexin, protein disulphide isomerase (PDI) and the ER oxidoreductase 1α (ERO1-Lα). A seven-fold rise in the levels of the transcription factor Chop along with an up-regulation of the active fragment at 42 kDa of caspase 12 completes the biochemical profile of the thapsigargin-treated neurones over their sixteen-hour stress course that signals for the engagement of the apoptotic phase of the UPR. The latter has been

further confirmed by the two-times increase in the proteolytic cleavage of caspase 3 [**Figures 8(j)**] and its downstream nuclear enzyme poly (ADP-ribose) polymerase (PARP) [**Figures 8(k)**] that both function as critical executioners of cell death (Chaitanya et al., 2010).

Two-way ANOVA demonstrates significant interactions between Liraglutide and thapsigargin on the protein levels of ATF6 ($F_{(1,28)} = 5.64$, $p = 0.0247$), the phosphorylated at Ser724 over the total Ire1α ($F_{(1,28)} = 13.38$, $p = 0.0010$), and of BiP ($F_{(1,28)} = 6.21$, $p = 0.0189$). Liraglutide co-treatment restores the down-regulated expression of full-length ATF6 and activity of Ire1α, as illustrated in **Figures 1(a)–1(b)**. It significantly ameliorates the abnormal BiP levels (*post-hoc*; $p \leq 0.01$) of the ER-stressed neurons [**Figure 1(c)**]. It further normalises the aberrant expression of calnexin [**Figure 1(d)**], Ero1-Lα [**Figure 1(e)**], and PDI [**Figure 1(f)**] to favour folding processes within the organelle lumen that altogether correlate with a significantly decreased neuronal Chop (two-way ANOVA interaction: $F_{(1,28)} = 14.19$, $p = 0.0008$) and cleaved caspase 3 content (two-way ANOVA interaction: $F_{(1,28)} = 10.06$, $p = 0.0037$) following ER stress [**Figures 1(g) & 8(j)**]. The proteolytic cleavage of caspase 12 and PARP, though, remains unaffected following Liralgutide co-treatment under chronic ER stress conditions, as shown in **Figures 1(h) & 8(k)**.

Similarly, the dual agonist reinstates homeostasis for the UPR effectors (two-way ANOVA interaction of dual agonist × thapsigargin: BiP, $F_{(1,28)} = 16.80$, $p = 0.0003$; ATF6, $F_{(1,28)} = 13.66$, $p = 0.0009$; Ire1α, $F_{(1,28)} = 18.12$, $p = 0.0002$) and molecular chaperones for ER function (two-way ANOVA interaction of dual agonist × thapsigargin: calnexin, $F_{(1,28)} = 10.66$, $p = 0.0029$; Ero1-Lα, $F_{(1,28)} = 7.70$, $p = 0.0097$; PDI, $F_{(1,28)} = 9.28$, $p = 0.0050$) upon chronic thapsigargin co-treatment [**Figure 1**]. The dual stimulation of GLP-1 and GIP receptors becomes notably essential for the resolution of the UPR, evident by the BiP normalisation [**Figure 1(c)**] in the ER-stressed neurones, when compared to the single GLP-1 activation (two-way ANOVA interaction of GIP receptor co-stimulation × thapsigargin: $F_{(1,28)} = 4.798$, $p = 0.0370$; *post hoc*, $p < 0.01$). It is additionally more critical for mitigating UPR apoptotic signals in neurones; the dual incretin produces a more considerable amelioration of the ectopic Chop expression [**Figure 1(g)**] when compared to Liraglutide (two-way ANOVA interaction of GIP receptor co-stimulation × thapsigargin: $F_{(1,28)} = 5.732$, $p = 0.0236$). It also brings back to control levels the expression of the cleaved caspases 3 [**Figure 8(j)**] and 12 [**Figure 1(h)**] and of the cleaved PARP [**Figure 8(k)**] upon irreversible ER stress.

3.2. GLP-1/GIP dual agonist balances the aberrant bioenergetics and mitochondrial function to the maximum.

Chronic ER stress with thapsigargin or tunicamycin generates a slow though persistent calcium flux into the mitochondria that provokes the aberrant membrane permeabilisation of the organelle (Deniaud et al., 2008). The latter perturbs the electrochemical gradient for $\Delta\Psi_m$ that orchestrates the respiratory rate, ATP synthesis and formation of reactive oxygen species, to potentiate a bioenergetic crisis and mitochondrial dysfunction (Rossi et al., 2019). As evident in our findings too, persistent ER stress with thapsigargin specifically dissipates the basal and maximal OCR that signals for mitochondrial respiration arrest and renders the neurones incapable and inflexible to meet their energy demands both under baseline and metabolically-challenging conditions [**Figure 2**]. It decreases by 6-fold the basal and compensatory glycolysis, signifying a shutdown of the anaerobic bioenergetic function, as well [**Figure 3**]. At the same time, it induces a four-times rise in the ratio of the aggregated over the monomer forms of JC1 [**Figure 4(a)**], indicating an exacerbation of the negative charge within the mitochondrial lumen.

Liraglutide co-treatment significantly ameliorates the suppressed basal respiration (two-way

ANOVA interaction: $F_{(1,11)} = 15.38$, $p = 0.0024$), maximal respiration (two-way ANOVA interaction: $F_{(1,11)} = 5.497$, $p = 0.0389$) and spare respiratory capacity (two-way ANOVA interaction: $F_{(1,11)} = 3.55$, $p = 0.05$) in chronically thapsigargin-stress neurones [**Figures 2(a)–2(b)**]. It attenuates the reduced basal glycolytic rate (two-way ANOVA main effect: $F_{(1,11)} = 9.33$, $p = 0.011$), basal PER (two-way ANOVA main effect: $F_{(1,11)} = 8.36$, $p = 0.015$) and compensatory glycolytic rate (two-way ANOVA main effect: $F_{(1,11)} = 10.24$, $p = 0.0085$) that parallel the fold decrease in the aggregated-over-monomer JC1 ratio, as respectively shown in **Figures 3** and **4(a)**.

The dual incretin similarly re-initiates the arrested oxidative phosphorylation (two-way ANOVA interaction of dual agonist × thapsigargin: basal OCR, $F_{(1,12)} = 10.18$, $p = 0.0078$; maximal OCR, $F_{(1,12)} = 8.045$, $p = 0.0150$; spare OCR, $F_{(1,12)} = 5.552$, $p = 0.0363$) [**Figure 2**] and glycolysis (two-way ANOVA main effect: basal glycolysis, $F_{(1,11)} = 10.83$, $p = 0.0072$; basal PER, $F_{(1,11)} = 19.47$, $p = 0.001$; compensatory glycolysis, $F_{(1,11)} = 12.52$, $p = 0.0046$) [**Figure 3**] in the thapsigargin-treated neurones. At the same time, it reduces by more than half the ratio of the aggregated to the monomeric forms of JC1, corresponding to an approximate normalisation of the values. Notably, the co-stimulation of GLP-1 and GIP receptors maximise the beneficial effect of the incretin treatment for the regulation of the $\Delta\Psi_m$ under conditions of persistent ER stress (two-way ANOVA interaction: $F_{(1,86)} = 9.931$, $p = 0.0022$), as illustrated in **Figure 4(a)**, which may further underlie the trend of the superior effect in oxidative metabolism and anaerobic cycling of glucose noted in **Figures 2(b)** and **3(b)**.

Mechanistically, the mitochondrial membrane permeabilisation for cell fate, the functional fidelity of the electron transport chain for mitochondrial respiration, and the import of metabolites in the mitochondrial lumen all integrate into the availability and activation patterns of selected Bcl-2-family members, such as Bcl-2, BAD, and BID (Bhola and Letai, 2016; Giménez-Cassina and Danial, 2015). With these regards, we have quantified functional phosphorylation of Bcl-2 at the serine 70 (Ruvolo et al., 2001) residue and the expression of the full-length BID by Western blotting [**Figures 4(b)–4(c)**]. Chronic ER stress with thapsigargin halves the expression levels of the phosphorylated and total Bcl-2 that signal for a notable inhibition of this protein. It further down-regulates the expression of full-length BID by 70%, indicative of its truncation into the active pro-apoptotic form (Upton et al., 2008). ELISA-based protein microarray additionally revealed that persistent SERCA favours the de-phosphorylation of BAD [**Figures 8(d)**] that, in turn, can bind and inhibit the pro-survival molecules Bcl-x_L, Bcl-2, and Bcl-W (Bhola and Letai, 2016; Giménez-Cassina and Danial, 2015). Incretin co-treatments normalise the suppressed expression of the full-length BID (two-way ANOVA interaction of Liraglutide × thapsigargin: $F_{(1,28)} = 23.50$, $p < 0.0001$; two-way ANOVA interaction of dual agonist × thapsigargin: $F_{(1,28)} = 19.47$, $p = 0.0001$), as illustrated in **Figure 4(c)**. Incretin co-treatments additionally restore the aberrant phosphorylation of BAD at the serine 112 residue (two-way ANOVA interaction of Liraglutide × thapsigargin: $F_{(1,28)} = 15.98$, $p = 0.0004$; two-way ANOVA interaction of dual agonist × thapsigargin: $F_{(1,28)} = 5.985$, $p = 0.0210$) back to basal levels [**Figure 8(d)**]. Liraglutide co-treatment ameliorates the aberrant inhibition of Bcl-2 under conditions of irreversible ER stress (two-way ANOVA interaction: $F_{(1,28)} = 4.573$, $p = 0.0413$), while the GLP-1/GIP dual agonist maximises the beneficial effect of incretin co-treatment on the function and availability of this Bcl-2-family member for survival signalling and oxidative phosphorylation (two-way ANOVA interaction of dual agonist × thapsigargin: $F_{(1,28)} = 17.93$, $p = 0.0002$; two-way ANOVA interaction of GIP-receptor co-stimulation × thapsigargin *vs.* GLP-1 mono-stimulation: $F_{(1,28)} = 8.498$, $p = 0.0069$), as shown in **Figure 4(b)**.

Next, we explored the hypothesis of whether the incretin-driven restored respiration could have been partially attributed to the enhanced mitochondrial biogenesis under ER stress conditions, as well. We quantified the expression ratio of the main sub-unit of complex IV, COX1 over the sub-unit A of respiratory complex II, SDH-A with a kinetic ELISA-based assay, as illustrated in **Figure 5(a)**. We initially observed that the chronic thapsigargin treatment detrimentally affects chromophore development over time (three-way ANOVA interaction: $F_{(13,975)} = 23.74$, $p < 0.0001$) and renders a decrease at the endpoint values of the ratio by 30% [**Figure 5(b)**] that signifies suppressed mitochondrial biogenesis under conditions of persistent ER stress. Incretin co-treatments significantly improve the signal development over time (three-way ANOVA interaction of time × thapsigargin × Liraglutide: $F_{(13,975)} = 2.065$, $p = 0.0140$; time × thapsigargin × dual incretin: $F_{(13,975)} = 4.151$, $p < 0.0001$) that corresponds to a normalisation of the expression ratio of the mitochondrial over the nuclear DNA-encoded complex sub-unit, as shown in **Figure 5**. Taken together, redressing the balance for mitochondria formation along with the restoration of bioenergetic regulators and pathways described earlier, points towards the beneficial engagement of GIP and/or GLP-1 receptors for maintaining metabolically-active neuronal cells in times of need.

3.3. Incretin co-treatments mitigate the autophagy arrest.

We have previously reported that the chronically persistent SERCA channel inhibition down-regulates major components for autophagosome formation and maturation and precludes the biogenesis of autophagic vacuoles in the neuroblastoma SH-SY5Y (Panagaki et al., 2017) and hepatoma HepG2 (Panagaki et al., 2020b) cell lines. Similarly, herein, we have observed that chronic thapsigargin treatment halves the neuronal expression of the autophagy-related (Atg) proteins beclin-1, Atg3, Atg7, and LC3B [**Figure 6**] that sequentially regulate the initiation of macro-autophagy (hereinafter called as autophagy), the downstream elongation and maturation of the autophagosome (Senft and Ronai, 2015). Liraglutide co-treatment restores the suppressed expression of beclin-1 (two-way ANOVA interaction: $F_{(1,28)} = 25.76$, $p \leq 0.001$), Atg3 (two-way ANOVA interaction: $F_{(1,28)} = 19.69$, $p = 0.0001$), Atg7 (two-way ANOVA interaction: $F_{(1,28)} = 28.21$, $p \leq 0.001$), and LC3 (two-way ANOVA interaction: $F_{(1,28)} = 9.815$, $p = 0.004$), as illustrated in **Figure 6**. Similarly, the dual incretin normalises the aberrant protein levels of beclin-1 (two-way ANOVA interaction: $F_{(1,28)} = 25.68$, $p \leq 0.001$), Atg3 (two-way ANOVA interaction: $F_{(1,28)} = 23.14$, $p \leq 0.001$), Atg7 (two-way ANOVA interaction: $F_{(1,28)} = 17.86$, $p = 0.0002$), and LC3 (two-way ANOVA interaction: $F_{(1,28)} = 5.483$, $p = 0.0265$) in the neurones subjected to chronic ER stress [**Figure 6**]. No superior efficacy of the dual incretin, when compared to Liraglutide (three-way ANOVA interaction of Atg proteins × thapsigargin × GIP-receptor co-stimulation: $F_{(3,112)} = 0.3943$, $p = 0.7574$), became apparent in the different regulators/components of the autophagic machinery.

3.4. Incretin co-treatments allay the synaptic and neuronal cell death.

Following, we asked how rectifying the aberrant ER-mitochondrial-autophagic axis could have affected synaptic and neuronal-cell fate. As prominent in our findings in **Figures 7(a)–7(b)**, the dual incretin reverts the suppressed expression the hallmark scaffolding protein for dendritic spine morphogenesis and synaptic plasticity, PSD95 (two-way ANOVA interaction: $F_{(1,28)} = 33.40$, $p < 0.0001$), and of the major pre-synaptic vesicle protein, synaptophysin (two-way ANOVA interaction: $F_{(1,28)} = 4.661$, $p = 0.0396$) to control levels upon chronic thapsigargin co-treatment. It further hinders the exacerbated LDH release into the supernatant (two-way ANOVA interaction: $F_{(1,101)} = 9.563$, $p = 0.0026$) that is indicative of constraining necrosis [**Figure 7(d)**], while it ameliorates the decreased XTT metabolisation (two-way ANOVA interaction: $F_{(1,92)} = 25.09$,

$p < 0.0001$), suggestive of switching neuronal towards survival under conditions of persistent ER stress [**Figure 7(c)**]. Liraglutide similarly normalises the reduced PSD95 (two-way ANOVA interaction: $F_{(1,28)} = 23.493$, $p < 0.0001$) and synaptophysin levels (two-way ANOVA interaction: $F_{(1,28)} = 6.83$, $p = 0.0142$) and attenuates the increased apoptosis (two-way ANOVA interaction for XTT: $F_{(1,92)} = 5.343$, $p = 0.023$) and necrosis (two-way ANOVA interaction for LDH: $F_{(1,108)} = 10.91$, $p = 0.0013$) of the neurone following chronic thapsigargin co-treatment, though with a pattern of a slightly restricted efficacy when compared to dual incretin, as shown in **Figure 7**.

3.5. Incretin co-treatments re-engage STAT3, Akt and Nrf2 signalling to preclude neuronal degeneration.

We have previously reported that the mono-activation of GLP-1 receptor re-instates homeostasis of the signal transducer and activator of transcription 3 (Stat3) and Akt signalling pathways to pave the way for normal cell proliferation and viability following chronic ER stress in the neuroblastoma SH-SY5Y cell line (Panagaki et al., 2017). Herein, we employed the same ELISA-based protein microarray [**Figure S1**] as in the study mentioned above to confirm/examine whether the incretin co-treatments regulates the same inter-cellular pathways in human post-mitotic neurones under conditions of chronic perturbation of the ER-mitochondrial-autophagic axis [**Figure 8** & **Table S2**]. Both Liraglutide and DA–CH3 mitigate the suppressed expression of the activating phosphorylation of STAT3 at the tyrosine residue 705 [**Figure 8(b)**] and Akt at the serine 473 and threonine 308 residues [**Figure 8(a)**] in post-mitotic neurones chronically challenged with 100 nM of thapsigargin. The co-stimulation of GIP receptor, though, maximises the beneficial of GLP-1 receptor in restoring activation patterns of Akt and Stat3 kinases under conditions of chronic ER stress. This rectification of the Akt kinase activation corresponds to a significant amelioration of the reduced phosphorylated levels of the proline-rich Akt substrate of 40 kDa (PRAS40) kinase at Thr246 ($p \leq 0.001$) and the mammalian target of rapamycin (mTOR) at Ser2448 ($p \leq 0.001$), with the DA–CH3 exerting rather better efficacy in relieving mTOR inhibition following chronic ER stress [**Figure 8(e)–8(f)**]. The latter is further accompanied by a prominent improvement of the 60%-reduced ribosomal protein S6 (rpS6) ($p \leq 0.001$) in post-mitotic neurones chronically challenged with 100 nM of thapsigargin, with Liraglutide normalising its phosphorylated levels.

Besides, chronic ER stress impedes the phosphorylation of the stress-responsive p53 [**Figure 8(i)**] and heat shock protein 27 (HSP27) [**Figure 8(h)**] at Ser15 ($p \leq 0.01$) and Ser78 ($p \leq 0.001$), respectively, whilst engaging the glycogen synthase kinase 3β [GSK3β; **Figure 8(c)**] by halving the inhibitory phosphorylation of the kinase at the serine 9 residue ($p \leq 0.001$). Liraglutide restores the expression of the phosphorylated p53 back to control levels and ameliorates the suppressed phosphorylation of HSP27 and GSK3β, though their levels have remained significantly decreased when compared to control conditions ($p \leq 0.05$). DA–CH3 co-treatment normalises the derailed neuronal GSK3β [**Figure 8(c)**], p53 [**Figure 8(i)**] and HSP27 [**Figure 8(h)**] activity under chronic thapsigargin treatment, signifying for a superior efficacy of the dual incretin over Liraglutide in rectifying inter-cellular signalling upon chronic ER stress.

Finally, we performed immunocytochemical analysis of the nuclear levels of the nuclear factor erythroid-derived 2-like 2 (Nrf2) to evaluate the antioxidant defensive signalling for neuroprotection upon aberrant proteostasis following chronic thapsigargin treatment [**Figure 9**]. Normally, Nrf2 is expressed throughout the neurone soma with a predominant expression in the nucleus (Ramsey et al., 2007), as prominent in our immunocytochemical analysis too [**Figure 9(a)**]. Contrarily, degenerating neurones feature a decreased nuclear Nrf2 content that signifies the impaired activity of the transcription factor (Ramsey et al., 2007). Accordingly, herein, thapsigargin-treated neurones

display a faint Nrf2-immunopositive staining, particularly in the nuclear area [**Figure 9(a)**]. One-way ANOVA analysis demonstrated significant differences in the nuclear Nrf2 content among the groups [$F_{(5,192)} = 4.635$, $p \leq 0.001$]. Two-way ANOVA analysis revealed that Liraglutide [$F_{(1,122)} = 11.57$, $p \leq 0.001$] and the DA–CH3 [$F_{(1,128)} = 17.30$, $p \leq 0.001$] co-treatments significantly modulate the Nrf2 nuclear content and notably normalise it, as illustrated in **Figure 9(b)**.

4. Discussion

Chronic ER stress has emerged as a hub for the derailed proteostasis underlying the onset and progression of neuronal degeneration, with the UPR and autophagy deregulation paralleling the temporal and spatial pattern of the pathologic protein deposition in human brain (Cai et al., 2016; Hetz and Mollereau, 2014; Ohno, 2017; Pereira, 2013; Santos and Ferreira, 2017). Chronic ER stress disproportionately impacts the signalling dynamics of the PERK, ATF6 and Ire1α branches to determine cell fate (Hetz et al., 2015; Lin et al., 2007). It suppresses ATF6 and Ire1α signalling (Li et al., 2010; Lin et al., 2007) to possibly attenuate the downstream survival signals and the neurotrophic effects of the spliced X-box binding protein 1(XBP-1) (Hetz et al., 2015). Spliced XBP1 regulates the transcription of the brain-derived neurotrophic factor (BDNF) and other genes related to the BDNF signalling to fine-tune synaptic plasticity in the murine hippocampus (Martínez et al., 2016). Accordingly, we show that chronic perturbation of ER calcium diminishes the phosphorylation of Ire1α at Ser724 and the expression of ATF6 that correlate to a decrease in the plasticity-related proteins, PSD95 and synaptophysin. Additionally, Ire1α activation is a prerequisite for initiating pro-survival autophagy in response to ER stress (Ogata et al., 2006). It mediates the phosphorylation of Bcl-2 to favour the dissociation of beclin-1 from its inhibitory complex with Bcl-2 at the ER membrane (Liu et al., 2016). It also stimulates the transcription factor XBP1 that in turn bounds to the promoter of beclin-1 and induces its transcription (Margariti et al., 2013). Herein, we show that post-mitotic neurones feature the suppressed Ire1α and Bcl-2 activity following irremediable ER stress that may account for the observed beclin-1 deficiency. For instance, a substantial loss of beclin-1 has been detected in the mid-frontal cortex of Alzheimer's patients that parallels disease progression (Pickford et al., 2008). Genetic depletion of beclin-1, furthermore, exacerbates amyloid β (Aβ) pathology and dampens the expression of synaptophysin, the dendrite-specific microtubule-associated protein 2 (MAP2) and of the calcium-binding protein, calbindin to potentiate synapse degeneration *in vivo* (Pickford et al., 2008).

Contrarily to Ire1α, chronic ER stress augments the activity of PERK to amplify and sustain the expression of the short-lived, pro-apoptotic transcription factor Chop (Lin et al., 2007). Chop inhibits the expression of the pro-survival Bcl-2 factor whilst stimulating the transcription of the ERO1-Lα to provoke the mitochondrial apoptotic machinery and neuronal damage (Hetz and Mollereau, 2014; Hetz et al., 2015), as prominent in our findings too. ERO1-Lα harnesses the oxidising power of the molecular oxygen to oxidise the active cysteinyl-thiol groups in PDI, enabling the latter to introduce disulphide bonds to folding substrates and to maintain the thiol-disulphide exchange and PDI capacity for the bond isomerisation within nascent polypeptides (Bulleid and Ellgaard, 2011). The redox fidelity of the oxidoreductase and the detoxification of the hydrogen peroxide produced upon the formation of a disulphide bond relies on the glutathione metabolism (Bulleid and Ellgaard, 2011) that is contingent on the Nrf2 activity (Pajares et al., 2017). Herein, we show the ERO1α excess correlates to PDI deficiency and a decreased Nrf2 nuclear (active) content, signalling for defective oxidative folding and high ER content of hydrogen peroxide. The latter along with the observed down-regulation of calnexin can exacerbate the abnormal protein load within the

organelle lumen to exacerbate the ER stress magnitude and hasten cell demise (Bousette et al., 2014; Zanotto-Filho et al., 2016). In addition, high levels of hydrogen peroxide drives the activation of the inositol-1,4,5-trisphosphate receptor (IP_3R) and increases the levels of calcium on the cytosolic face of the ER. The latter along with the deficiency of calnexin that normally regulates the retrieval of the release calcium to the ER perturbs the calcium availability into the mitochondrion (Simmen et al., 2010). Aberrant calcium dynamics limit mitochondrial respiration, whilst inducing the core apoptosis machinery (Kaufman and Malhotra, 2014) and the proteolytic (activating) cleavage of CASP12 (Nakagawa and Yuan, 2000). Active CASP12 potentiates a downstream caspase cascade (*e.g.*, CASP3) that mediates synaptophysin depletion and executes PARP degradation to assure the fulfilment and irreversibility of the apoptotic process for synapse and neuronal toxicity (Kitamura et al., 2003; Morishima et al., 2002; Mungarro-Menchaca et al., 2002; Nakagawa et al., 2000; Quiroz-Baez et al., 2011), as reflected in our results too. Besides the modulation of redox signalling and core apoptosis machinery, CHOP can obscure autophagy through the transcriptional regulation of Atg components for phagophore elongation and maturation into the autophagosome, including the Atg7 gene (B'chir et al., 2013, 2014). Atg7 deficiency potentiates a spontaneous accumulation of protein aggregates, neuronal degeneration and loss *in vivo* (Komatsu et al., 2006).

Liraglutide and dual incretin co-treatments both alleviate the ectopic BiP and CHOP expressions, rectify the aberrant IRE1α, Nrf2 and CASP12 activity, and restore the protein levels of ATF6, PDI, calnexin, ERO1-Lα, beclin-1, Atg3, Atg7, and LC3. These biochemical traits correspond to the an amelioration of the suppressed oxidative phosphorylation and glycolysis and mitochondrial hyperpolarisation. They additionally correlate with the normalisation of PSD95 and synaptophysin expression and restraint of the aberrant neuronal toxicity in the XTT-assessed metabolic activity assay, LDH levels and the proteolysis of the executioner CASP3 and PARP. Our results collectively suggest that the incretin mimetics shift the 'terminal' signals of UPR into adaptive that favours the homeostasis of autophagy, mitochondrial and quality control machinery. This in turn abets the proteostasis, cell bioenergetics, and neuronal repair following persistent ER stress, with the GIP receptor co-stimulation maximising the neuroprotective effect of the GLP-1 receptor.

Mechanistically, the incretin mimetics restore the suppressed STAT3 and Akt signalling to elicit neuroprotection upon persistent ER stress. STAT3 is a latent transcription factor that lies downstream the stimulation of cytokine and growth factor receptors, including the GLP-1 receptor (Shiraishi et al., 2012). Suppressed STAT3 activity occurs in the hippocampus of affected patients and animals of Alzheimer's disease (Chiba et al., 2008). Chiba *et al.* have demonstrated that Aβ inactivates the hippocampal JAK2 (Janus kinase 2)/STAT3 axis to compromise basal forebrain cholinergic function and induce spatial working memory deficits *in vivo*, linking the STAT3 pathway to neurodegenerative processes (Chiba et al., 2008). Subsequent work has further revealed that the ER stress perturbs the astrocytic STAT3 signalling to modulate acute-phase neuroinflammatory responses in a PERK-dependent fashion (Meares et al., 2014). Although the mechanistic interplay between the UPR and STAT3 signalling in the context of neuronal functioning and fate remains elusive, STAT3 regulates the transcription of the pro-survival Bcl-2 protein and axonal outgrowth/branching programs to promote neuronal survival and axonal regeneration post oxygen-glucose deprivation and excitotoxicity (Chen et al., 2016; Park et al., 2012). Activated STAT3 additionally induces the expression of synaptophysin that enhances synaptogenesis and synaptic plasticity in the hippocampus and cortex (Chen et al., 2016; ClaireDominique et al., 2007). As such, the restoration of STAT3 activation may offer a node through which GLP-1 and GIP receptors confer trophic signals for the synapse homeostasis and neuronal repair following chronic ER

stress.

Akt is a serine/threonine kinase with a wide spectrum of targets in the cytoplasm, nucleus, mitochondria, and the ER membrane to regulate adaptive responses and cell fate under stress conditions (Manning and Toker, 2017). Herein, we show Liraglutide and the dual incretin alleviate the ER stress-induced inhibition of Akt phosphorylation at Thr308 and Ser473 sites, signalling for rescuing its maximal activity (Manning and Toker, 2017). The latter corresponds to an amelioration of the suppressed phosphorylation of PRAS40 at Thr246 and thus relieves the PRAS40 inhibition of the mTOR signalling (Haar et al., 2007). The importance of this observation lies on the fact that the mTOR signalling positively regulates protein synthesis, ribosomal biogenesis, oxidative metabolism and mitochondrial function (Laplante and Sabatini, 2009). ER stress derails mTOR activity and renders neurones vulnerable to CHOP/ERO1α-mediated oxidative damage; as such it facilitates the intrinsic apoptotic machinery (Di Nardo et al., 2009), as reflected in our findings too. Suppressed mTOR has been previously reported to underlie the down-regulated expression of the activity-regulated cytoskeleton-associated protein (Arc) for synaptic plasticity and the impaired long-term potentiation in degenerating murine hippocampus (Heras-Sandoval et al., 2014). Suppressed mTOR further abolishes the inhibitory phosphorylation of Atg13 and unc-51-like kinase 1 (ULK1) that allow the formation of the ULK complex and the induction of autophagy (Heras-Sandoval et al., 2014; Laplante and Sabatini, 2009). However, excessive autophagic flux degrades endogenous inhibitors of apoptosis and Atg components and detrimentally affects cell fate (Heras-Sandoval et al., 2014; Shuling et al., 2017).

In contrast to the mTOR kinase, Akt phosphorylates and inhibits GSK3β that critically drives neuronal apoptosis following ER stress (Brewster et al., 2006; Meares et al., 2011; Panagaki et al., 2017; Song et al., 2002; Takadera et al., 2007). In the degenerating brain, GSK3β immunoreactive granules occur in neurones with activated PERK signalling (Hoozemans et al., 2009; Nijholt et al., 2013). Activated PERK engages GSK3β activity through selective removal of the inactive (phosphorylated at Ser9) kinase form via the autosomal-lysosomal pathway (Nijholt et al., 2013). GSK3β in turn inhibits Nrf2 by nuclear exclusion and proteosomal degradation that could preclude the transcription of genes for oxidative folding (Pajares et al., 2017) and mitochondrial biogenesis (Gureev et al., 2019). Intriguingly, active (nuclear) Nrf2 also induces the expression of regulatory proteins for the autophagy initiation, cargo recognition, autophagosome formation, elongation and autolysosome clearance (Pajares et al., 2016, 2017) whilst precluding the recruitment of ATF4 to the CHOP promoter and thereby CHOP transcription (Zong et al., 2012). In addition, Akt phosphorylates and inhibits the death-agonist BAD, which becomes rapidly de-phosphorylated upon apoptotic stimuli (Manning and Cantley, 2007). The restoration of BAD phosphorylation, through Akt, raises the mitochondrial threshold for apoptosis and renders cells less vulnerable to death signals (Datta et al., 2002), as prominent in our results too. Akt can further phosphorylate the stress-responsive HSP27 (Chen et al., 2015) that sequesters cytochrome c and/or pro-caspase 3 to preclude the apoptosome formation and downstream death signal transduction (Bakthisaran et al., 2015; Benn et al., 2002; Stetler et al., 2012). Furthermore, activated HSP27 phosphorylates p53 at Ser15 and induces its downstream target gene expression to prevent genototoxicity (Bakthisaran et al., 2015; Xu et al., 2013). Lastly, activated Akt may also phosphorylate and inhibit PERK kinase (Mounir et al., 2011), offering an additional mechanistic link for the neuroprotective and restorative effects of incretin mimetics upon persistent ER stress. Exacerbated PERK activity triggers general translation repression and down-regulation of the plasticity-related cyclic AMP response-element-binding protein (CREB), through its downstream targets eIF2α and ATF4 respectively, to provoke PSD95

deficiency, synapse damage and cognitive decline *in vivo* (Ohno, 2017). Although we have not assessed the expression of phosphorylated PERK levels, transcriptional and translational regulation of Chop expression primarily lies downstream of the PERK arm (Lin et al., 2007). Taken together, our findings suggest that the stimulation of GIP and/or GLP-1 receptors rectify Akt activation to counteract the ER stress-driven suppression of mTOR and HSP27 signalling and to hamper the exacerbated GSK3β activity. These effects, in turn, normalise Nrf2 nuclear levels and reinforce trophic signals upon chronic ER stress for neuronal survival and availability of the major synaptic proteins, PSD95 and synaptophysin.

5. Conclusion

In conclusion, our study demonstrates the neuroprotective and restorative effects of Liraglutide and the novel dual incretin upon persistent ER stress in human neurones, confirming our current knowledge of their neuro-pharmacological effects (Hölscher, 2018). It additionally broadens the spectrum of intercellular functions, processes, and responses that the GIP and/or GLP-1 receptors can modulate in human neurones. Notably, in a pilot clinical trial, Liraglutide has rescued the decline of cerebral glucose consumption in Alzheimer's patients, indicative of improved energy metabolism in brain areas correlated with cognitive decline and disease progression (Gejl et al., 2016). These encouraging results have led to a randomised, placebo-controlled, double-blind phase II clinical trial of Liraglutide in Alzheimer's cases (Hölscher, 2018) of which the results are expected soon. Our present findings provide translational data for paving the way for re-purposing these traditionally anti-diabetic therapeutic agents to the clinical management of degenerative disorders and abet their burden in society.

Author contributions

Conceptualisation, C.H. and T.P.; methodology, T.P. and E.B.R.; formal analysis, T.P. and E.B.R.; investigation, T.P. and E.B.R.; resources, C.H. and C.S..; data curation, T.P., E.B.R., C.H., and C.S.; writing–original draft preparation, T.P.; writing–review and editing, T.P., E.B.R., C.H., and C.S.; visualization, T.P. and E.B.R.; supervision, C.H. and C.S.; project administration, C.H.; funding acquisition, C.H..

Acknowledgements

We would like to acknowledge the Rosetrees Trust, UK and Alzheimer's Research Society, UK for financially supporting our research.

Conflict of Interest Statement

C.H. is a named inventor on several patent applications for the use of incretin mimetics as treatments for neurodegenerative disorders. Rest authors declare no competing interests.

References

R. Bakthisaran, R. Tangirala, and C. M. Rao. Small heat shock proteins: Role in cellular functions and pathology. *Biochimica et Biophysica Acta (BBA) – Proteins and Proteomics*, 1854(4):291–319, 2015.

W. B'chir, A.-C. Maurin, V. Carraro, J. Averous, C. Jousse, Y. Muranishi, L. Parry, G. Stepien, P. Fafournoux, and A. Bruhat. The eIF2α/ATF4 pathway is essential for stress-induced autophagy gene expression. *Nucleic Acids Research*, 41(16):7683, 2013.

W. B'chir, C. Chaveroux, V. Carraro, J. Averous, A.-C. Maurin, C. Jousse, Y. Muranishi, L. Parry, P. Fafournoux, and A. Bruhat. Dual role for CHOP in the crosstalk between autophagy and apoptosis to determine cell fate in response to amino acid deprivation. *Cellular Signalling*, 26(7):1385–1391, 2014.

S. C. Benn, D. Perrelet, A. C. Kato, J. Scholz, I. Decosterd, R. J. Mannion, J. C. Bakowska, and C. J. Woolf. Hsp27 Upregulation and Phosphorylation Is Required for Injured Sensory and Motor Neuron Survival. *Neuron*, 36(1): 45–56, 2002.

P. D. Bhola and A. Letai. Mitochondria-judges and executioners of cell death sentences. *Mol Cell*, 61(5):695–704, 2016.

N. Bousette, C. Abbasi, R. Chis, and A. O. Gramolini. Calnexin silencing in mouse neonatal cardiomyocytes induces Ca^{2+} cycling defects, er stress, and apoptosis. *journal of Cellular Physiology*, 229(3):374–383, 2014.

R. Bravo, J. M. Vicencio, V. Parra, R. Troncoso, J. P. Munoz, M. Bui, C. Quiroga, A. E. Rodriguez, H. E. Verdejo, J. Ferreira, M. Iglewski, M. Chiong, T. Simmen, A. Zorzano, J. A. Hill, B. A. Rothermel, G. Szabadkai, and S. Lavandero. Increased er–mitochondrial coupling promotes mitochondrial respiration and bioenergetics during early phases of er stress. *Journal of Cell Science*, 124(13):2143–2152, 2011.

J. Brewster, D. Linseman, R. Bouchard, F. Loucks, T. Precht, E. Esch, and K. Heidenreich. Endoplasmic reticulum stress and trophic factor withdrawal activate distinct signaling cascades that induce glycogen synthase kinase-3β and a caspase-9-dependent apoptosis in cerebellar granule neurons. *Molecular and Cellular Neuroscience*, 32(3): 242 –253, 2006.

N. J. Bulleid and L. Ellgaard. Multiple ways to make disulfides. *Trends in Biochemical Sciences*, 36(9):485–492, 2011.

Y. Cai, J. Arikkath, L. Yang, M.-L. Guo, P. Periyasamy, and S. Buch. Interplay of endoplasmic reticulum stress and autophagy in neurodegenerative disorders. *Autophagy*, 12(2):225–244, 2016.

G. V. Chaitanya, A. J. Steven, and P. P. Babu. PARP-1 cleavage fragments: signatures of cell-death proteases in neurodegeneration. *Cell communication and signaling : CCS*, 8:31, 2010.

H. Chen, W. Lin, Y. Zhang, L. Lin, J. Chen, Y. Zeng, M. Zheng, Z. Zhuang, H. Du, R. Chen, and N. Liu. IL-10 Promotes Neurite Outgrowth and Synapse Formation in Cultured Cortical Neurons after the Oxygen-Glucose Deprivation via JAK1/STAT3 Pathway. *Scientific Reports*, 6(30459):1–16, 2016.

H.-F. Chen, S.-J. Liu, and G. Chen. Heat shock protein 27 phosphorylation in the proliferation and apoptosis of human umbilical vein endothelial cells induced by high glucose through the phosphoinositide-3 kinase/Akt and extracellular signal regulated kinase 1/2 pathways. *Molecular medicine reports*, 11(2):1504–1508, 2015.

T. Chiba, M. Yamada, J. Sasabe, K. Terashita, M. Shimoda, M. Matsuoka, and S. Aiso. Amyloid-β causes memory impairment by disturbing the JAK2/STAT3 axis in hippocampal neurons. *Mol Psychiatry*, 14(2):206–222, 2008.

W. ClaireDominique, L. Hong, W. Sylvain, and R. Denis. Long?lasting effects of elevated neonatal leptin on rat hippocampal function, synaptic proteins and NMDA receptor subunits. *Journal of Neuroscience Research*, 85(4): 816–828, 2007.

S. R. Datta, A. M. Ranger, M. Z. Lin, J. F. Sturgill, Y.-C. Ma, C. W. Cowan, P. Dikkes, S. J. Korsmeyer, and M. E. Greenberg. Survival factor-mediated bad phosphorylation raises the mitochondrial threshold for apoptosis. *Developmental Cell*, 3(5):631–643, 2002.

A. Deniaud, O. Sharaf el dein, E. Maillier, D. Poncet, G. Kroemer, C. Lemaire, and C. Brenner. Endoplasmic reticulum stress induces calcium-dependent permeability transition, mitochondrial outer membrane permeabilization and apoptosis. *Oncogene*, 27(3):285–299, 2008.

A. Di Nardo, I. Kramvis, N. Cho, A. Sadowski, L. Meikle, D. J. Kwiatkowski, and M. Sahin. Tuberous Sclerosis Complex Activity is Required to Control Neuronal Stress Responses in an mTOR-Dependent Manner. *The Journal of Neuroscience*, 29(18):5926–5937, 2009.

B. Finan, T. Ma, N. Ottaway, T. D. Müller, K. M. Habegger, K. M. Heppner, H. Kirchner, J. Holland, J. Hembree, C. Raver, S. H. Lockie, D. L. Smiley, V. Gelfanov, B. Yang, S. Hofmann, D. Bruemmer, D. J. Drucker, P. T. Pfluger, D. Perez-Tilve, J. Gidda, L. Vignati, L. Zhang, J. B. Hauptman, M. Lau, M. Brecheisen, S. Uhles, W. Riboulet, E. Hainaut, E. Sebokova, K. Conde-Knape, A. Konkar, R. D. DiMarchi, and M. H. Tschöp. Unimolecular dual incretins maximize metabolic benefits in rodents, monkeys, and humans. *Science Translational Medicine*, 5(209): 1–8, 2013.

J. R. Friedman, L. L. Lackner, M. West, J. R. DiBenedetto, J. Nunnari, and G. K. Voeltz. Er tubules mark sites of mitochondrial division. *Science*, 334(6054):358–362, 2011.

M. Gejl, A. Gjedde, L. Egefjord, A. Møller, S. B. Hansen, K. Vang, A. Rodell, H. Brændgaard, H. Gottrup, A. Schacht, N. Møller, B. Brock, and J. Rungby. In Alzheimer's Disease, 6-Month Treatment with GLP-1 Analog Prevents Decline of Brain Glucose Metabolism: Randomized, Placebo-Controlled, Double-Blind Clinical Trial. *Frontiers in Aging Neuroscience*, 8:108, 2016.

A. Giménez-Cassina and N. N. Danial. Regulation of mitochondrial nutrient and energy metabolism by bcl-2 family proteins. *Trends Endocrinol Metab*, 26(4):165–175, 2015.

A. P. Gureev, E. A. Shaforostova, and V. N. Popov. Regulation of mitochondrial biogenesis as a way for active longevity: Interaction between the nrf2 and PGC-1α signaling pathways. *Frontiers in Genetics*, 10:435, 2019.

E. V. Haar, S.-i. Lee, S. Bandhakavi, T. J. Griffin, and D.-H. Kim. Insulin signalling to mTOR mediated by the Akt/PKB substrate PRAS40. *Nature Cell Biology*, 9(3):316–323, 2007.

D. Heras-Sandoval, J. M. Pérez-Rojas, J. Hernández-Damián, and J. Pedraza-Chaverri. The role of PI3K/AKT/mTOR pathway in the modulation of autophagy and the clearance of protein aggregates in neurodegeneration. *Cellular Signalling*, 26(12):2694–2701, 2014.

C. Hetz and B. Mollereau. Disturbance of endoplasmic reticulum proteostasis in neurodegenerative diseases. *Nat Rev Neurosci*, 15(4):233–49, 2014.

C. Hetz, E. Chevet, and S. A. Oakes. Proteostasis control by the unfolded protein response. *Nat Cell Biol*, 17: 829–838, 2015.

C. Hölscher. Novel dual GLP-1/GIP receptor agonists show neuroprotective effects in Alzheimer's and Parkinson's disease models. *Neuropharmacology*, *In Press*, 2018.

J. J. Hoozemans, E. S. van Haastert, D. A. Nijholt, A. J. Rozemuller, P. Eikelenboom, and W. Scheper. The unfolded protein response is activated in pretangle neurons in alzheimer's disease hippocampus. *Am J Pathol*, 174 (4):1241–51, 2009.

R. J. Kaufman and J. D. Malhotra. Calcium trafficking integrates endoplasmic reticulum function with mitochondrial bioenergetics. *Biochimica et Biophysica Acta (BBA) - Molecular Cell Research*, 1843(10):2233–2239, 2014.

Y. Kitamura, A. Miyamura, K. Takata, M. Inden, D. Tsuchiya, K. Nakamura, and T. Taniguchi. Possible involvement of both endoplasmic reticulum-and mitochondria-dependent pathways in thapsigargin-induced apoptosis in human neuroblastoma sh-sy5y cells. *journal of Pharmacological Sciences*, 92(3):228–236, 2003.

M. Komatsu, S. Waguri, T. Chiba, S. Murata, J.-i. Iwata, I. Tanida, T. Ueno, M. Koike, Y. Uchiyama, E. Kominami, and K. Tanaka. Loss of autophagy in the central nervous system causes neurodegeneration in mice. *Nature*, 441: 880–884, 2006.

E. Korkotian and M. Segal. Fast confocal imaging of calcium released from stores in dendritic spines. *European Journal of Neuroscience*, 10(6):2076–2084, 1998.

F. Korobova, V. Ramabhadran, and H. N. Higgs. An actin-dependent step in mitochondrial fission mediated by the er-associated formin inf2. *Science*, 339(6118):464–467, 2013.

N. T. Ktistakis. ER platforms mediating autophagosome generation. *Biochimica et Biophysica Acta (BBA) - Molecular and Cell Biology of Lipids*, 1865(1):158433, 2020.

M. Laplante and D. M. Sabatini. mTOR signaling at a glance. *Journal of Cell Science*, 122(20):3589–3594, 2009.

H. Li, A. V. Korennykh, S. L. Behrman, and P. Walter. Mammalian endoplasmic reticulum stress sensor ire1 signals by dynamic clustering. *Proceedings of the National Academy of Sciences*, 107(37):16113–16118, 2010.

J. H. Lin, H. Li, D. Yasumura, H. R. Cohen, C. Zhang, B. Panning, K. M. Shokat, M. M. LaVail, and P. Walter. IRE1 signaling affects cell fate during the unfolded protein response. *Science*, 318(5852):944–949, 2007.

D. Liu, X. Liu, T. Zhou, W. Yao, J. Zhao, Z. Zheng, W. Jiang, F. Wang, F. O. Aikhionbare, D. L. Hill, N. Emmett, Z. Guo, D. Wang, X. Yao, and Y. Chen. IRE1–RACK1 axis orchestrates ER stress preconditioning-elicited cytoprotection from ischemia/reperfusion injury in liver. *journal of Molecular Cell Biology*, 8(2):144, 2016.

J. Lotharius, S. Barg, P. Wiekop, C. Lundberg, H. K. Raymon, and P. Brundin. Effect of mutant α-synuclein on dopamine homeostasis in a new human mesencephalic cell line. *Journal of Biological Chemistry*, 277(41): 38884–38894, 2002.

J. Lotharius, J. Falsig, J. van Beek, S. Payne, R. Dringen, P. Brundin, and M. Leist. Progressive degeneration of human mesencephalic neuron-derived cells triggered by dopamine-dependent oxidative stress is dependent on the mixed-lineage kinase pathway. *Journal of Neuroscience*, 25(27):6329–6342, 2005.

B. D. Manning and L. C. Cantley. AKT/PKB signaling: Navigating downstream. *Cell*, 129(7):1261–1274, 2007.

B. D. Manning and A. Toker. AKT/PKB Signaling: Navigating the Network. *Cell*, 169(3):381–405, 2017.

A. Margariti, H. Li, T. Chen, D. Martin, G. Vizcay-Barrena, S. Alam, E. Karamariti, Q. Xiao, A. Zampetaki, Z. Zhang, W. Wang, Z. Jiang, C. Gao, B. Ma, Y.-G. Chen, G. Cockerill, Y. Hu, Q. Xu, and L. Zeng. Xbp1 mrna

splicing triggers an autophagic response in endothelial cells through BECLIN-1 transcriptional activation. *journal of Biological Chemistry*, 288(2):859–872, 2013.

G. Martínez, R. Vidal, P. Mardones, F. Serrano, A. Ardiles, C. Wirth, P. Valdés, P. Thielen, B. Schneider, B. Kerr, J. Valdés, A. Palacios, N. Inestrosa, L. Glimcher, and C. Hetz. Regulation of Memory Formation by the Transcription Factor XBP1. *Cell Reports*, 14(6):1382–1394, 2016.

G. Martínez, C. Duran-Aniotz, F. Cabral-Miranda, J. P. Vivar, and C. Hetz. Endoplasmic reticulum proteostasis impairment in aging. *Aging Cell*, 16(4):615–623, 2017.

G. Martínez, S. Khatiwada, M. Costa-Mattioli, and C. Hetz. ER proteostasis control of neuronal physiology and synaptic function. *Trends in Neurosciences*, 41(9):610–624, 2018.

G. P. Meares, M. A. Mines, E. Beurel, T.-Y. Eom, L. Song, A. A. Zmijewska, and R. S. Jope. Glycogen synthase kinase-3 regulates endoplasmic reticulum (ER) stress-induced CHOP expression in neuronal cells. *Experimental Cell Research*, 317(11):1621–1628, 2011.

G. P. Meares, Y. Liu, R. Rajbhandari, H. Qin, S. E. Nozell, J. A. Mobley, J. A. Corbett, and E. N. Benveniste. PERK-dependent activation of JAK1 and STAT3 contributes to endoplasmic reticulum stress-induced inflammation. *Molecular and Cellular Biology*, 34(20):3911–3925, 2014.

B. Mellström and J. R. Naranjo. Mechanisms of Ca^{2+}-dependent transcription. *Current Opinion in Neurobiology*, 11(3):312–319, 2001.

N. Morishima, K. Nakanishi, H. Takenouchi, T. Shibata, and Y. Yasuhiko. An endoplasmic reticulum stress-specific caspase cascade in apoptosis: Cytochrome c-independent activation of caspase-9 by caspase-12. *journal of Biological Chemistry*, 277(37):34287–34294, 2002.

Z. Mounir, J. L. Krishnamoorthy, S. Wang, B. Papadopoulou, S. Campbell, W. J. Muller, M. Hatzoglou, and A. E. Koromilas. Akt determines cell fate through inhibition of the PERK-eIF2α phosphorylation pathway. *Science Signaling*, 4(192):ra62, 2011.

X. Mungarro-Menchaca, P. Ferrera, J. Morán, and C. Arias. β-Amyloid peptide induces ultrastructural changes in synaptosomes and potentiates mitochondrial dysfunction in the presence of ryanodine. *Journal of Neuroscience Research*, 68(1):89–96, 2002.

T. Nakagawa and J. Yuan. Cross-Talk between Two Cysteine Protease Families. *The Journal of Cell Biology*, 150 (4):887–894, 2000.

T. Nakagawa, H. Zhu, N. Morishima, E. Li, J. Xu, B. A. Yankner, and J. Yuan. Caspase-12 mediates endoplasmic-reticulum-specific apoptosis and cytotoxicity by amyloid-β. *Nature*, 403(6765):98–103, 2000.

D. A. T. Nijholt, A. Nölle, E. S. van Haastert, H. Edelijn, R. F. Toonen, J. J. M. Hoozemans, and W. Scheper. Unfolded protein response activates glycogen synthase kinase-3 via selective lysosomal degradation. *Neurobiology of Aging*, 34(7):1759–1771, 2013.

M. Ogata, S.-i. Hino, A. Saito, K. Morikawa, S. Kondo, S. Kanemoto, T. Murakami, M. Taniguchi, I. Tanii, K. Yoshinaga, S. Shiosaka, J. A. Hammarback, F. Urano, and K. Imaizumi. Autophagy is activated for cell survival after endoplasmic reticulum stress. *Molecular and Cellular Biology*, 26(24):9220–9231, 2006. doi: 10.1128/MCB.01453-06.

M. Ohno. PERK as a hub of multiple pathogenic pathways leading to memory deficits and neurodegeneration in Alzheimer's disease. *Brain Research Bulletin*, *In Press*, 2017.

M. Pajares, N. Jiménez-Moreno, Á. J. García-Yagüe, M. Escoll, M. L. de Ceballos, F. Van Leuven, A. Rábano, M. Yamamoto, A. I. Rojo, and A. Cuadrado. Transcription factor NFE2L2/NRF2 is a regulator of macroautophagy genes. *Autophagy*, 12(10):1902–1916, 2016.

M. Pajares, A. Cuadrado, and A. I. Rojo. Modulation of proteostasis by transcription factor NRF2 and impact in neurodegenerative diseases. *Redox Biology*, 11:543–553, 2017.

T. Panagaki, M. Michael, and C. Hölscher. Liraglutide restores chronic ER stress, autophagy impairments and apoptotic signalling in SH-SY5Y cells. *Scientific Reports*, 7(1):16158, 2017.

T. Panagaki, E. B. Randi, and C. Szabo. Role of 3-mercaptopyruvate sulfurtransferase in the regulation of proliferation and cellular bioenergetics in human Down Syndrome fibroblasts. *Biomolecules*, 10(4):653, 2020a.

T. Panagaki, E. B. Randi, and C. Szabo. Role of hydrogen sulfide and 3-mercaptopyruvate sulfurtransferase in the regulation of the endoplasmic reticulum stress response in hepatocytes. *Biomolecules*, 10(12):1692, 2020b.

K. W. Park, S. E. Nozell, and E. N. Benveniste. Protective Role of STAT3 in NMDA and Glutamate-Induced Neuronal Death: Negative Regulatory Effect of SOCS3. *PLOS ONE*, 7(11):e50874, 2012.

C. M. Pereira. Crosstalk between endoplasmic reticulum stress and protein misfolding in neurodegenerative diseases. *ISRN Cell Biology*, 2013:22, 2013.

S. W. Perry, J. P. Norman, J. Barbieri, E. B. Brown, and H. A. Gelbard. Mitochondrial membrane potential probes and the proton gradient: a practical usage guide. *BioTechniques*, 50(2):98–115, 2011.

F. Pickford, E. Masliah, M. Britschgi, K. Lucin, R. Narasimhan, P. A. Jaeger, S. Small, B. Spencer, E. Rockenstein,

B. Levine, and T. Wyss-Coray. The autophagy-related protein beclin 1 shows reduced expression in early Alzheimer disease and regulates amyloid β accumulation in mice. *The Journal of Clinical Investigation*, 118(6):2190–2199, 2008.

R. Quiroz-Baez, P. Ferrera, R. Rosendo-Gutierrez, J. Moran, F. Bermudez-Rattoni, and C. Arias. Caspase-12 activation is involved in amyloid-β protein-induced synaptic toxicity. *J Alzheimers Dis*, 26(3):467–76, 2011.

O. A. Ramírez and A. Couve. The endoplasmic reticulum and protein trafficking in dendrites and axons. *Trends Cell Biol*, 21(4):219–227, 2011.

C. P. Ramsey, C. A. Glass, M. B. Montgomery, K. A. Lindl, G. P. Ritson, L. A. Chia, R. L. Hamilton, C. T. Chu, and K. L. Jordan-Sciutto. Expression of Nrf2 in neurodegenerative diseases. *J Neuropathol Exp Neurol*, 66(1): 75–85, 2007.

A. Rossi, P. Pizzo, and R. Filadi. Calcium, mitochondria and cell metabolism: A functional triangle in bioenergetics. *Biochim Biophys Acta Mol Cell Res*, 1866(7):1068–1078, 2019.

P. Ruvolo, X. Deng, and W. May. Phosphorylation of bcl2 and regulation of apoptosis. *Leukemia*, 15(4):515–522, 2001.

L. E. Santos and S. T. Ferreira. Crosstalk between endoplasmic reticulum stress and brain inflammation in Alzheimer's disease. *Neuropharmacology, In Press*, 2017.

D. Scholz, D. Pöltl, A. Genewsky, M. Weng, T. Waldmann, S. Schildknecht, and M. Leist. Rapid, complete and large-scale generation of post-mitotic neurons from the human LUHMES cell line. *Journal of Neurochemistry*, 119 (5):957–971, 2011.

M. Schroder and R. J. Kaufman. The mammalian unfolded protein response. *Annu Rev Biochem*, 74:739–89, 2005.

D. Senft and Z. A. Ronai. Upr, autophagy, and mitochondria crosstalk underlies the er stress response. *Trends in Biochemical Sciences*, 40(3):141–148, 2015.

D. Shiraishi, Y. Fujiwara, Y. Komohara, H. Mizuta, and M. Takeya. Glucagon-like peptide-1 (GLP-1) induces M2 polarization of human macrophages via STAT3 activation. *Biochemical and Biophysical Research Communications*, 425(2):304–308, 2012.

S. Shuling, T. Jin, M. Yuyang, L. Mengmeng, and Z. Qiang. Crosstalk of autophagy and apoptosis: Involvement of the dual role of autophagy under ER stress. *Journal of Cellular Physiology*, 232(11):2977–2984, 2017.

T. Simmen, E. M. Lynes, K. Gesson, and G. Thomas. Oxidative protein folding in the endoplasmic reticulum: tight links to the mitochondria-associated membrane (MAM). *Biochim Biophys Acta*, 1798(8):1465–1473, 2010.

L. Song, P. De Sarno, and R. S. Jope. Central role of glycogen synthase kinase-3β in endoplasmic reticulum stress-induced caspase-3 activation. *J Biol Chem*, 277(47):44701–8, 2002.

R. A. Stetler, Y. Gao, L. Zhang, Z. Weng, F. Zhang, X. Hu, S. Wang, P. Vosler, G. Cao, D. Sun, S. H. Graham, and J. Chen. Phosphorylation of HSP27 by Protein Kinase D is Essential for Mediating Neuroprotection Against Ischemic Neuronal Injury. *The Journal of Neuroscience*, 32(8):2667–2682, 2012.

N. V. Stiegler, A. K. Krug, F. Matt, and M. Leist. Assessment of chemical-induced impairment of human neurite outgrowth by multiparametric live cell imaging in high-density cultures. *Toxicological Sciences*, 121(1):73–87, 2011.

G. E. Stutzmann and M. P. Mattson. Endoplasmic Reticulum Ca^{2+} Handling in Excitable Cells in Health and Disease. *Pharmacological Reviews*, 63(3):700–727, 2011.

T. Takadera, M. Fujibayashi, H. Kaniyu, N. Sakota, and T. Ohyashiki. Caspase-dependent apoptosis induced by thapsigargin was prevented by glycogen synthase kinase-3 inhibitors in cultured rat cortical neurons. *Neurochemical Research*, 32(8):1336–1342, 2007.

J.-P. Upton, K. Austgen, M. Nishino, K. M. Coakley, A. Hagen, D. Han, F. R. Papa, and S. A. Oakes. Caspase-2 cleavage of BID is a critical apoptotic signal downstream of endoplasmic reticulum stress. *Molecular and Cellular Biology*, 28(12):3943–3951, 2008.

Y. Wang, J. Shen, N. Arenzana, W. Tirasophon, R. J. Kaufman, and R. Prywes. Activation of atf6 and an atf6 dna binding site by the endoplasmic reticulum stress response. *Journal of Biological Chemistry*, 275(35):27013–27020, 2000.

Y. Xu, Y. Diao, S. Qi, X. Pan, Q. Wang, Y. Xin, X. Cao, J. Ruan, Z. Zhao, L. Luo, C. Liu, and Z. Yin. Phosphorylated Hsp27 activates ATM-dependent p53 signaling and mediates the resistance of MCF-7 cells to doxorubicin-induced apoptosis. *Cellular Signalling*, 25(5):1176–1185, 2013.

A. Zanotto-Filho, V. P. Masamsetti, E. Loranc, S. S. Tonapi, A. Gorthi, X. Bernard, R. M. Gonçalves, J. C. F. Moreira, Y. Chen, and A. J. R. Bishop. Alkylating AgentÐInduced NRF2 Blocks Endoplasmic Reticulum StressÐMediated Apoptosis via Control of Glutathione Pools and Protein Thiol Homeostasis. *Molecular Cancer Therapeutics*, 15(12):3000–3014, 2016.

Z.-H. Zong, Z.-X. Du, N. Li, C. Li, Q. Zhang, B.-Q. Liu, Y. Guan, and H.-Q. Wang. Implication of Nrf2 and ATF4

in differential induction of CHOP by proteasome inhibition in thyroid cancer cells. *Biochimica & Biophysica Acta (BBA) – Molecular Cell Research*, 1823(8):1395–1404, 2012.

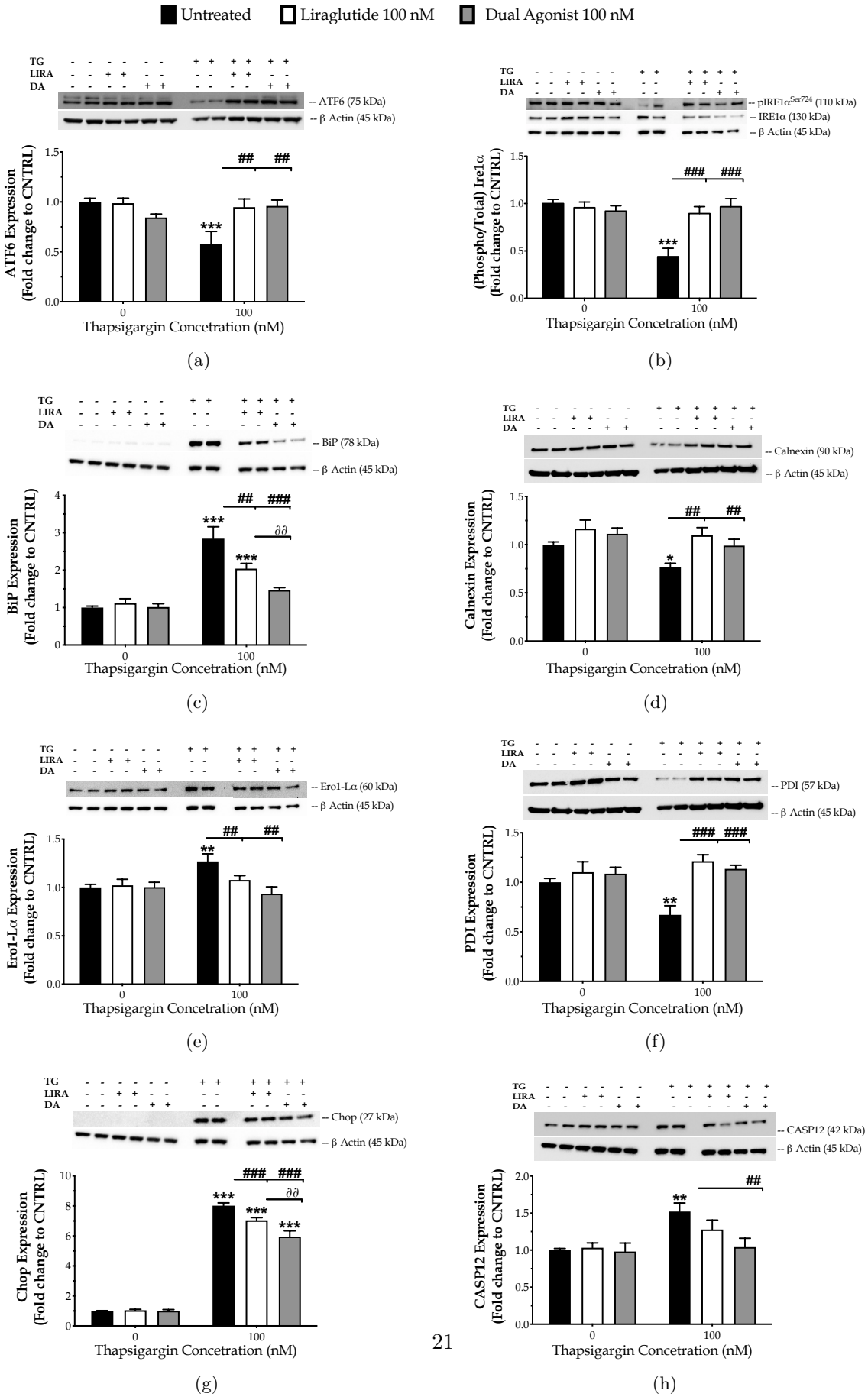
Untreated
Liraglutide 100 nM
Dual Agonist 100 nM
TG
LIRA
DA
-- ATF6 (75 kDa)
-- β Actin (45 kDa)
ATF6 Expression (Fold change to CNTRL)
Thapsigargin Concetration (nM)
(a)
-- pIRE1α Ser724 (110 kDa)
-- IRE1α (130 kDa)
-- β Actin (45 kDa)
(Phospho/Total) Ire1α (Fold change to CNTRL)
Thapsigargin Concetration (nM)
(b)
-- BiP (78 kDa)
-- β Actin (45 kDa)
BiP Expression (Fold change to CNTRL)
Thapsigargin Concetration (nM)
(c)
-- Calnexin (90 kDa)
-- β Actin (45 kDa)
Calnexin Expression (Fold change to CNTRL)
Thapsigargin Concetration (nM)
(d)
-- Ero1-Lα (60 kDa)
-- β Actin (45 kDa)
Ero1-Lα Expression (Fold change to CNTRL)
Thapsigargin Concetration (nM)
(e)
-- PDI (57 kDa)
-- β Actin (45 kDa)
PDI Expression (Fold change to CNTRL)
Thapsigargin Concetration (nM)
(f)
-- Chop (27 kDa)
-- β Actin (45 kDa)
Chop Expression (Fold change to CNTRL)
Thapsigargin Concetration (nM)
(g)
-- CASP12 (42 kDa)
-- β Actin (45 kDa)
CASP12 Expression (Fold change to CNTRL)
Thapsigargin Concetration (nM)
(h)

Figure 1: **Liraglutide (LIRA) and the GLP-1/GIP dual agonist (DA) both attenuate the neuronal unfolded protein response (UPR) and restore folding capacity within the endoplasmic reticulum (ER) lumen, with the dual activation of the GLP-1 and GIP receptors superiorly restoring the expression of apoptotic UPR mediators.** On d 6 of the differentiation period, post-mitotic neurones from the human LUHMES cell line were treated with 0 and 100 nM of thapsigargin (TG) in the presence or absence of each incretin tested for 16 h. Neurones were then harvested, and the expression of (i) the UPR transducers – ATF6 **[(a)]** and phosphorylated to total IRE1α **[(b)]**, (ii) the local chaperones BiP **[(c)]**, calnexin **[(d)]**, Ero1-Lα **[(e)]**, and (iii) of the UPR mediators for apoptotic signalling – Chop **[(g)]** and caspase 12 (CASP12) **[(h)]** were determined by Western blotting. β-Actin served as the loading control to our quantitative analyses. Each bar represents the mean ± SEM from five independent experiments. Data are expressed as fold change to the control (CNTRL; unstressed/untreated conditions) and analysed by two-way ANOVA, followed by *post hoc* Bonferroni's multiple comparison t-test: $^{*}p \leq 0.05$, $^{**}p \leq 0.01$ & $^{***}p \leq 0.001$ compared to CNTRL; $^{\sharp}p \leq 0.05$, $^{\sharp\sharp}p \leq 0.01$ & $^{\sharp\sharp\sharp}p \leq 0.001$ compared to the TG-stressed neurones; $^{\partial\partial}p \leq 0.01$ compared to the Liraglutide-treated, TG-stressed neurones.

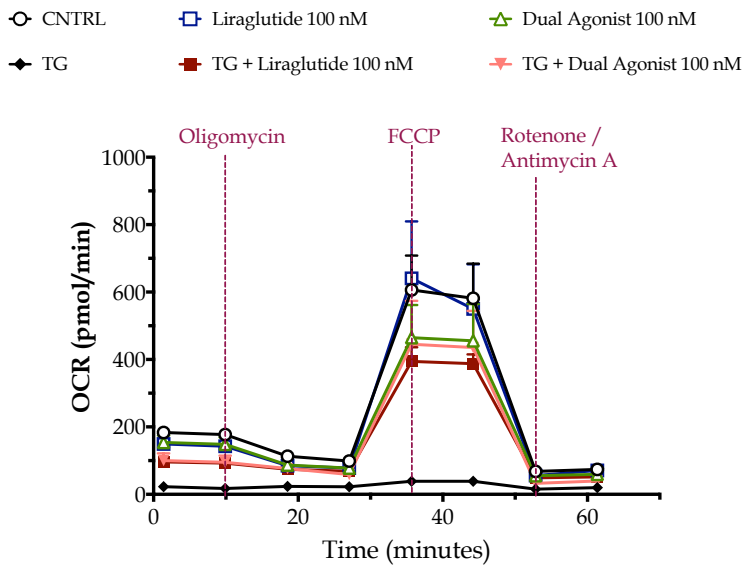
CNTRL
Liraglutide 100 nM
Dual Agonist 100 nM
TG
TG + Liraglutide 100 nM
TG + Dual Agonist 100 nM
Oligomycin
FCCP
Rotenone / Antimycin A
OCR (pmol/min)
Time (minutes)

(a)

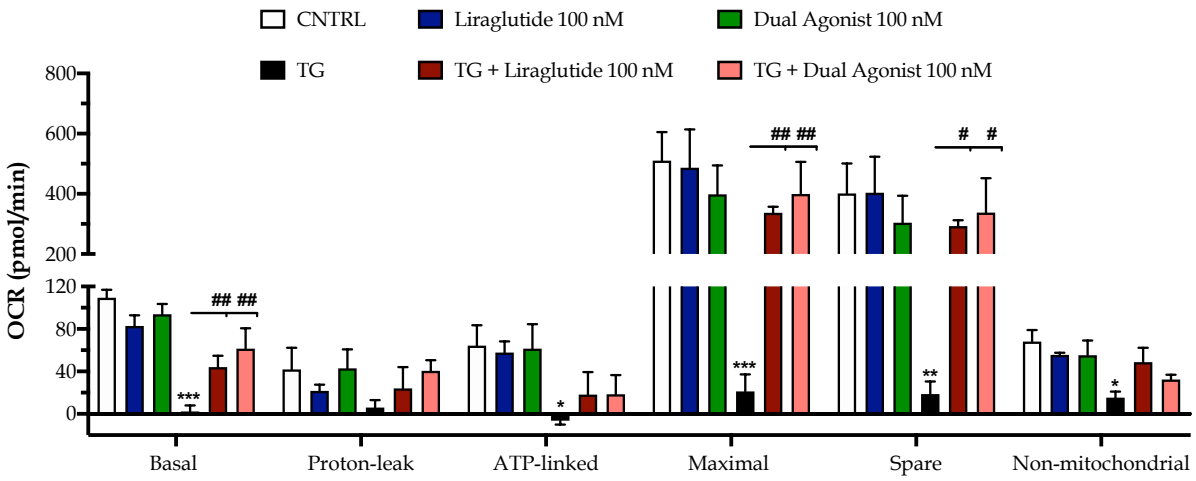
CNTRL
Liraglutide 100 nM
Dual Agonist 100 nM
TG
TG + Liraglutide 100 nM
TG + Dual Agonist 100 nM
OCR (pmol/min)
Basal
Proton-leak
ATP-linked
Maximal
Spare
Non-mitochondrial

(b)

Figure 2: **Liraglutide and the GLP-1/GIP dual agonist restore the arrested oxidative phosphorylation in neurones subjected to persistent ER stress.** On d 6 of the differentiation period, post-mitotic neurones from the human LUHMES cell line were treated with 0 and 100 nM of thapsigargin (TG) in the presence or absence of each incretin tested for 16 h. We then monitored the oxygen consumption rate (OCR) over the sequential injection of oligomycin (1 µM; ATP synthase inhibitor), FCCP (1.5 µM; mitochondrial uncoupler) and of Rotenone + Antimycin A (0.5 µM; complex I and III inhibitors) with the Seahorse XFe24 Extracellular Flux Analyzer, as illustrated in the representative profile for neuronal mitochondrial respiration **[(a)]**. Basal, ATP-linked, proton-leak, maximal and non-mitochondrial OCR were subsequently quantified and illustrated as bar graphs **[(b)]**. Each point and bar represent the mean ± SEM from five independent experiments. Data processed with two-way ANOVA, followed by *post hoc* Bonferroni's multiple comparison t-test: $^{*}p \leq 0.05$, $^{**}p \leq 0.01$ & $^{***}p \leq 0.001$ compared to the control (CNTRL; unstressed/untreated conditions); $^{\sharp}p \leq 0.05$ & $^{\sharp\sharp}p \leq 0.01$ compared to the TG-stressed neurones.

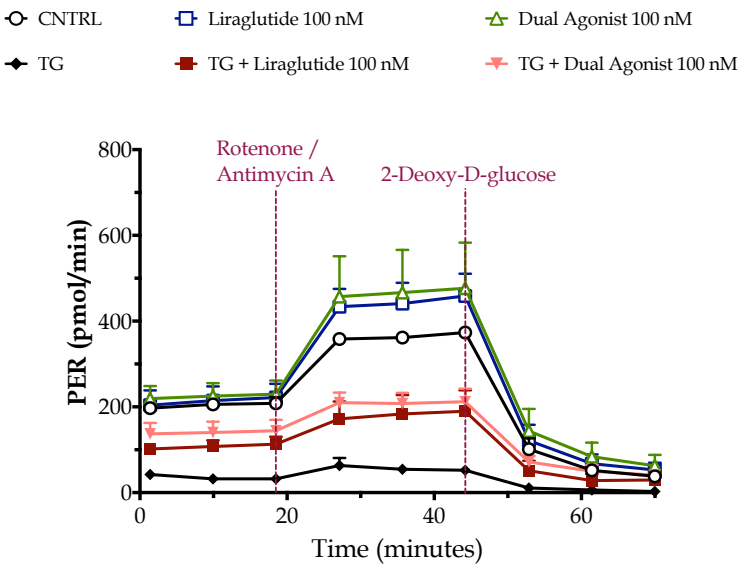
CNTRL
Liraglutide 100 nM
Dual Agonist 100 nM
TG
TG + Liraglutide 100 nM
TG + Dual Agonist 100 nM
Rotenone /
Antimycin A
2-Deoxy-D-glucose
PER (pmol/min)
800
600
400
200
0
0
20
40
60
Time (minutes)

(a)

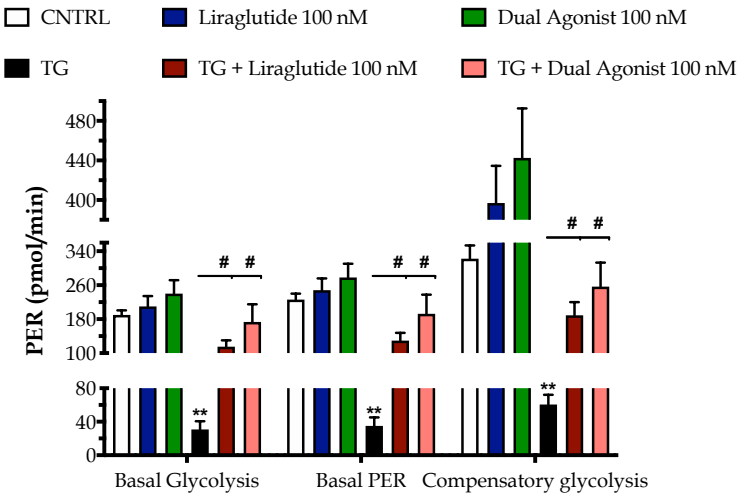
CNTRL
Liraglutide 100 nM
Dual Agonist 100 nM
TG
TG + Liraglutide 100 nM
TG + Dual Agonist 100 nM
PER (pmol/min)
480
440
400
340
260
180
100
80
40
0
# #
# #
# #
**
**
**
Basal Glycolysis
Basal PER
Compensatory glycolysis

(b)

Figure 3: **Incretin co-treatments re-balance the suppressed neuronal glycolysis under conditions of persistent ER stress.** On d 6 of the differentiation period, post-mitotic neurones from the human LUHMES cell line were treated with 0 and 100 nM of thapsigargin (TG) in the presence or absence of each incretin tested for 16 h. We then quantified the proton efflux rate (PER) over the sequential injection of Rotenone + Antimycin A (to compel the cells to rely on glycolysis for ATP production) and 2-deoxy-D-glucose (20 mM; to inhibit the glycolytic ATP production) with the Seahorse XFe24 Extracellular Flux Analyzer, as illustrated in the representative profile **[(a)]**. Basal glycolysis, basal PER, and compensatory glycolysis were subsequently calculated and illustrated as bar graphs **[(b)]**. Each point and bar represent the mean ± SEM from five independent experiments. Data processed with two-way ANOVA, followed by *post hoc* Bonferroni's multiple comparison t-test: $^{**}p \leq 0.01$ compared to the control (CNTRL; unstressed/untreated conditions); $^{\sharp}p \leq 0.05$ compared to the TG-stressed neurones.

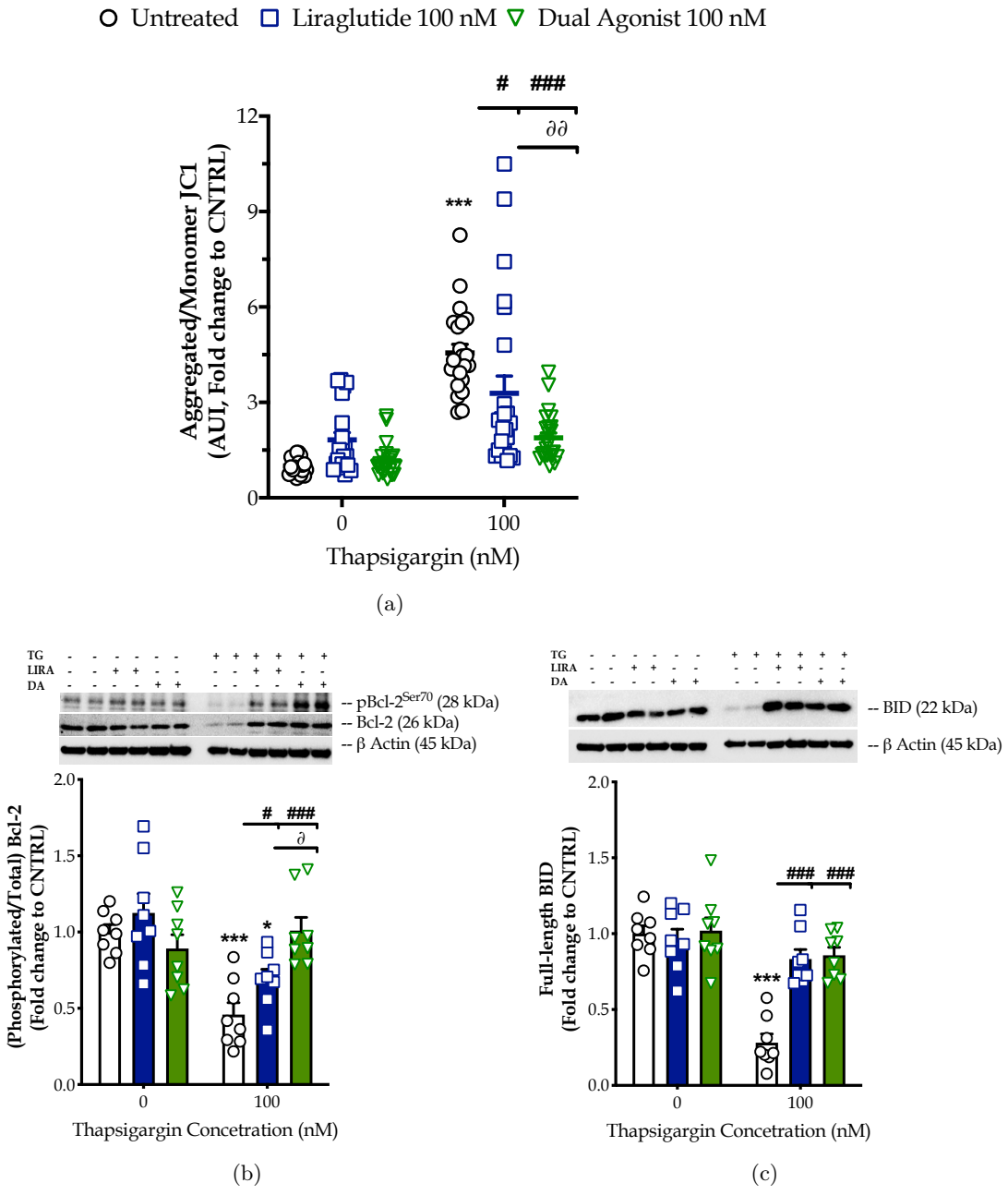
Untreated
Liraglutide 100 nM
Dual Agonist 100 nM
Aggregated/Monomer JC1
(AUI, Fold change to CNTRL)
Thapsigargin (nM)
(a)
TG
LIRA
DA
-- pBcl-2Ser70 (28 kDa)
-- Bcl-2 (26 kDa)
-- β Actin (45 kDa)
(Phosphorylated/Total) Bcl-2
(Fold change to CNTRL)
Thapsigargin Concetration (nM)
(b)
-- BID (22 kDa)
-- β Actin (45 kDa)
Full-length BID
(Fold change to CNTRL)
Thapsigargin Concetration (nM)
(c)

Figure 4: **The GLP-1/GIP dual agonist maximises the incretin-derived benefit on rescuing the hyperpolarisation of the mitochondrial membrane upon chronic neuronal ER stress.** On d 6 of differentiation period, post-mitotic neurones from the human LUHMES cell line were treated with 0 and 100 nM of thapsigargin in the presence or absence of each incretin tested for 16 h. We then probed the neurones with 20 µM JC-1 for 10 min and monitored the fluorescence signal of the aggregated over the monomer form of the dye in a microplate reader. Fluorescent signal (in arbitrary units – AUI) has been normalised to the corresponding (per condition) cell density (Janus Green staining). Each bar represents the mean ± SEM from five independent experiments. Data processed with two-way ANOVA, followed by *post hoc* Bonferroni's multiple comparison t-test: $^{***}p \leq 0.001$ compared to the control (CNTRL; unstressed/untreated conditions); $^{\sharp}p \leq 0.05$ & $^{\sharp\sharp\sharp}p \leq 0.001$ compared to the TG-stressed neurones; $^{\partial\partial}p \leq 0.01$ compared to the Liraglutide-treated, TG-stressed neurones.

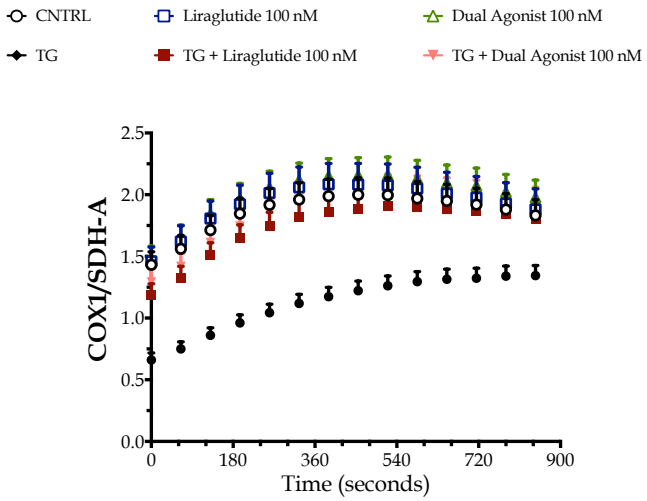
CNTRL
Liraglutide 100 nM
Dual Agonist 100 nM
TG
TG + Liraglutide 100 nM
TG + Dual Agonist 100 nM
COX1/SDH-A
2.5
2.0
1.5
1.0
0.5
0.0
0
180
360
540
720
900
Time (seconds)

(a)

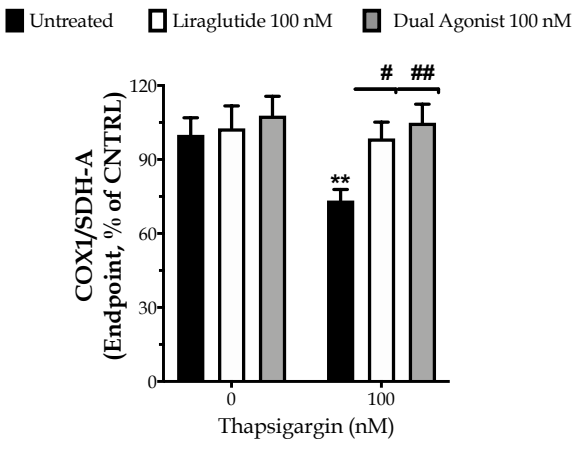
Untreated
Liraglutide 100 nM
Dual Agonist 100 nM
COX1/SDH-A
(Endpoint, % of CNTRL)
120
90
60
30
0
**
#
##
0
100
Thapsigargin (nM)

(b)

Figure 5: **Liraglutide and the GLP-1/GIP dual agonist mitigate the impaired mitochondrial biogenesis of neurones subjected to irreversible ER stress.** On d 6 of the differentiation period, post-mitotic neurones from the human LUHMES cell line were treated with 0 and 100 nM of thapsigargin (TG) in the presence or absence of each incretin tested for 16 h. Neurones were fixed with 4% paraformaldehyde and monitored for the protein expression ratio of the cytochrome c oxidase subunit I (COX1; mitochondrial DNA-encoded protein) to the succinate dehydrogenase (SDH-A; nuclear DNA-encoded protein) over a kinetic cycle of 15 min for signal development with a colourimetric ELISA assay **[(a)]**. Endpoint measurements of the ratio are expressed as percentages of the control (CNTRL; untreated/unstressed conditions) and illustrated as a bar graph **[(b)]**. Each point and bar represent the mean ± SEM from five independent experiments. Data processed with two-way ANOVA, followed by *post hoc* Bonferroni's multiple comparison t-test: $^{**}p \leq 0.01$ compared to the control (CNTRL; unstressed/untreated conditions); $^{\sharp}p \leq 0.05$ & $^{\sharp\sharp}p \leq 0.01$ compared to the TG-stressed neurones.

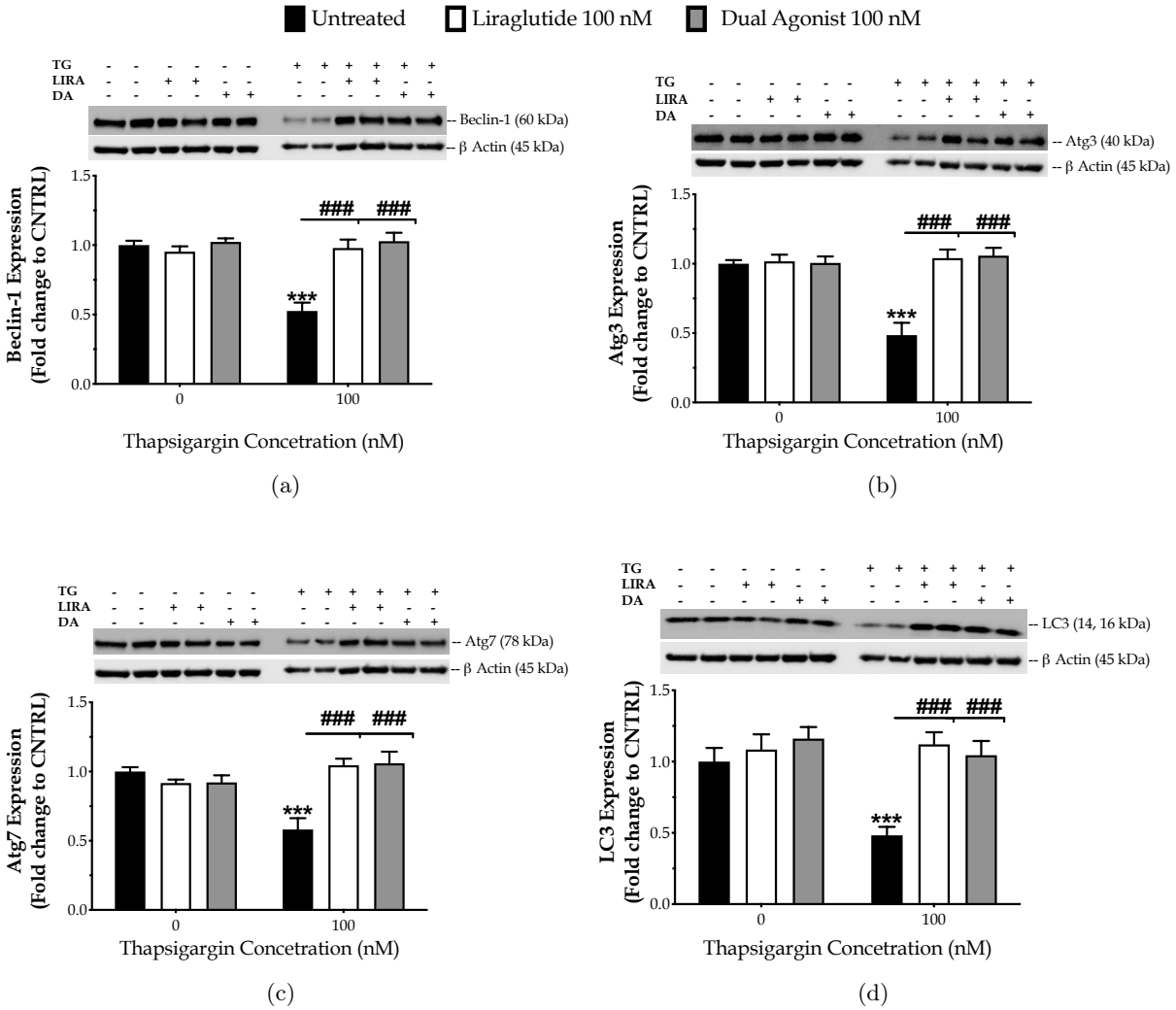
Untreated
Liraglutide 100 nM
Dual Agonist 100 nM
TG
LIRA
DA
-- Beclin-1 (60 kDa)
-- β Actin (45 kDa)
Beclin-1 Expression (Fold change to CNTRL)
###
***
Thapsigargin Concetration (nM)
(a)
-- Atg3 (40 kDa)
Atg3 Expression (Fold change to CNTRL)
(b)
-- Atg7 (78 kDa)
Atg7 Expression (Fold change to CNTRL)
(c)
-- LC3 (14, 16 kDa)
LC3 Expression (Fold change to CNTRL)
(d)

Figure 6: **Liraglutide (LIRA) and the GLP-1/GIP dual agonist (DA) normalise the suppressed expression of core autophagy-related proteins (Atg) proteins for autophagosome formation and maturation in neurones subjected to chronic ER stress.** On d 6 of the differentiation period, post-mitotic neurones from the LUHMES cell line were treated with 0 and 100 nM of thapsigargin (TG) in the presence or absence of each incretin tested for 16 h. Neurones were harvested, and the expression of beclin-1 **[(a)]**, Atg3 **[(b)]**, Atg7 **[(c)]** and of LC3 **[(d)]** were determined by Western blotting. β-Actin was used as the loading control in our quantification. Each bar represents the mean ± SEM from five independent experiments. Data expressed as fold change to the control (CNTRL; unstressed/untreated conditions) and processed with two-way ANOVA, followed by *post hoc* Bonferroni's multiple comparison t-test: $^{***}p \leq 0.001$ compared to CNTRL; $^{\sharp\sharp\sharp}p \leq 0.001$ compared to the TG-stressed neurones.

673

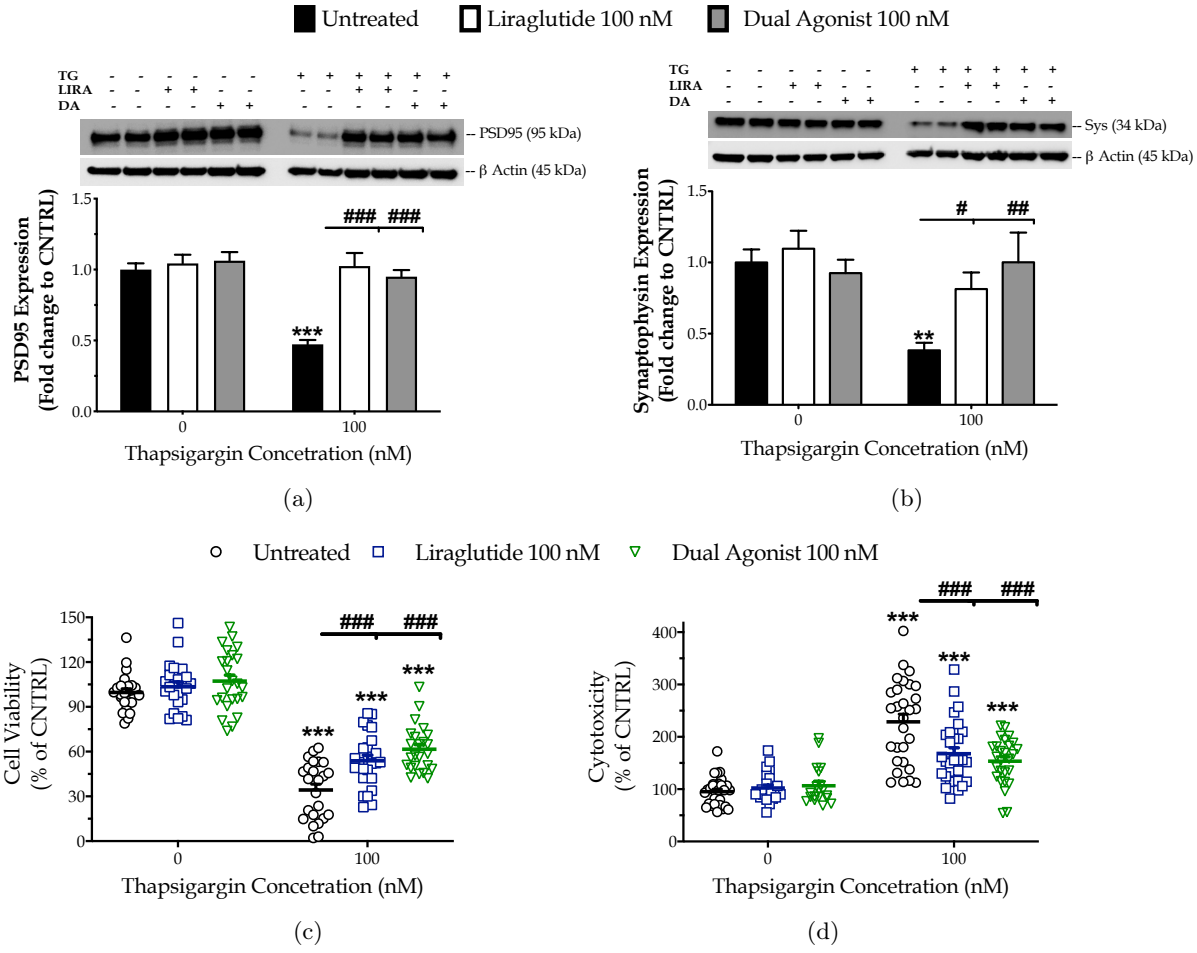
Untreated
Liraglutide 100 nM
Dual Agonist 100 nM
TG
LIRA
DA
-- PSD95 (95 kDa)
-- β Actin (45 kDa)
PSD95 Expression (Fold change to CNTRL)
Thapsigargin Concetration (nM)
(a)
-- Sys (34 kDa)
-- β Actin (45 kDa)
Synaptophysin Expression (Fold change to CNTRL)
Thapsigargin Concetration (nM)
(b)
Untreated
Liraglutide 100 nM
Dual Agonist 100 nM
Cell Viability (% of CNTRL)
Thapsigargin Concetration (nM)
(c)
Cytotoxicity (% of CNTRL)
Thapsigargin Concetration (nM)
(d)

Figure 7: **Incretin co-treatments allay the synaptic and neuronal-cell death upon irreversible ER stress.** On d 6 of the differentiation period, post-mitotic neurones from the LUHMES cell line were treated with 0 and 100 nM of thapsigargin (TG) in the presence or absence of 100 nM Liraglutide (LIRA) or of 100 nM novel GLP-1/GIP Dual Agonist (DA) for 16 h. Neurones were then harvested, and the expression of postsynaptic density protein 95 [PSD95; **(a)**] and synaptophysin [Sys; **(b)**] were determined by Western blotting. β-Actin was used as the loading control in our quantification. Alternatively, neurones were assayed for the XTT metabolisation [**(c)**] to assess cell viability. Spent supernatant was collected and processed for the LDH activity [**(d)**] to determine necrosis. Each bar or line represents mean ± SEM from five independent experiments. Data are expressed as fold change to the control (CNTRL; unstressed/untreated conditions) and processed with two-way ANOVA, followed by *post hoc* Bonferroni's multiple comparison t-test: $^{**}p \leq 0.01$ & $^{***}p \leq 0.001$ compared to CNTRL; $^{\sharp}p \leq 0.05$, $^{\sharp\sharp}p \leq 0.01$ & $^{\sharp\sharp\sharp}p \leq 0.001$ compared to the TG-stressed neurones.

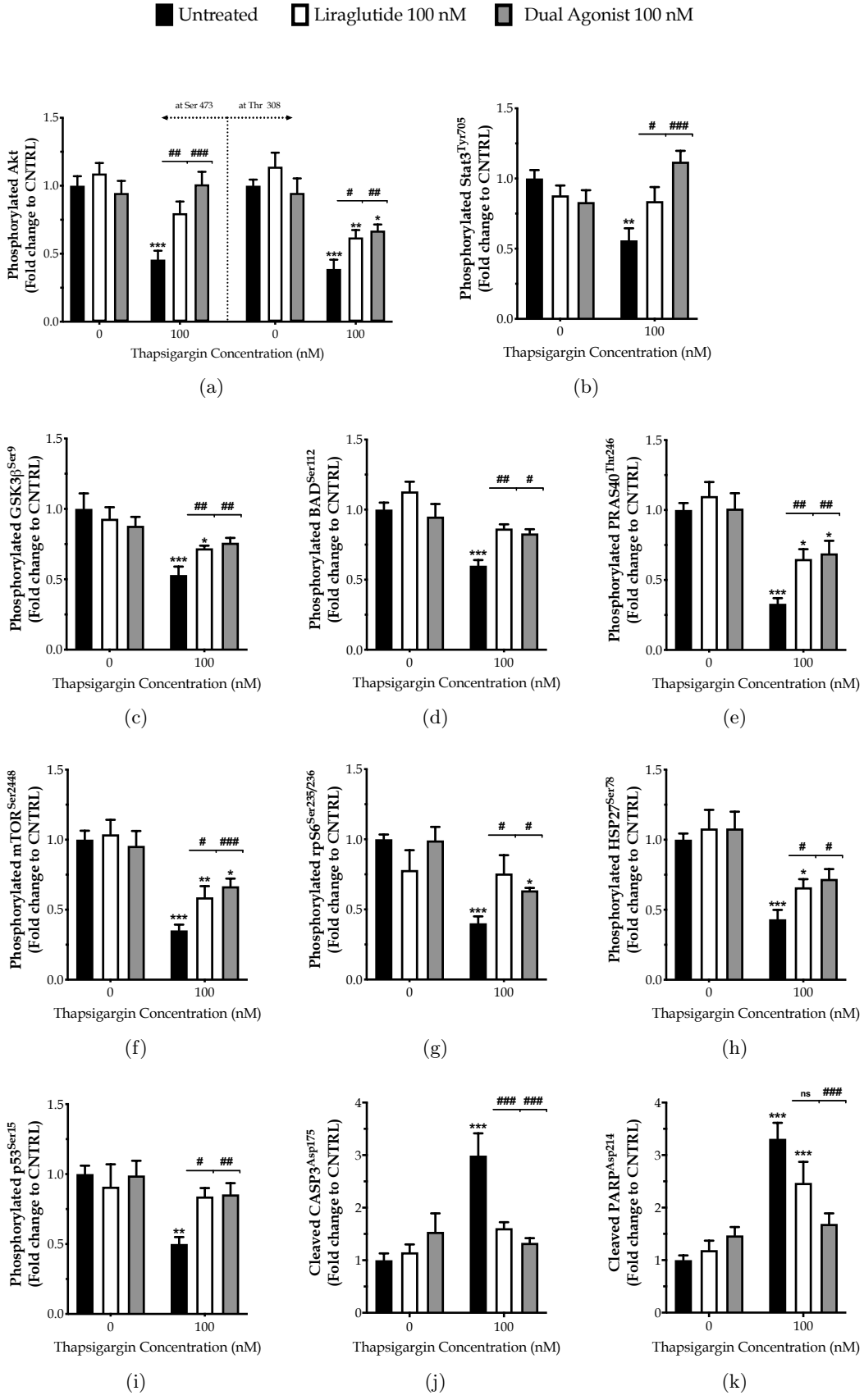
Untreated
Liraglutide 100 nM
Dual Agonist 100 nM
at Ser 473
at Thr 308
Phosphorylated Akt (Fold change to CNTRL)
Phosphorylated Stat3Tyr705 (Fold change to CNTRL)
Phosphorylated GSK3β Ser9 (Fold change to CNTRL)
Phosphorylated BADSer112 (Fold change to CNTRL)
Phosphorylated PRAS40Thr246 (Fold change to CNTRL)
Phosphorylated mTORSer2448 (Fold change to CNTRL)
Phosphorylated rpS6Ser235/236 (Fold change to CNTRL)
Phosphorylated HSP27Ser78 (Fold change to CNTRL)
Phosphorylated p53Ser15 (Fold change to CNTRL)
Cleaved CASP3Asp175 (Fold change to CNTRL)
Cleaved PARPAsp214 (Fold change to CNTRL)
Thapsigargin Concentration (nM)
(a)
(b)
(c)
(d)
(e)
(f)
(g)
(h)
(i)
(j)
(k)

Figure 8: **Incretin co-treatments restore the derailed Akt and Stat3 intercellular signalling to halt the ectopic poly (ADP-ribose) polymerase (PARP) and caspase 3 (CASP3) cleavage, balance the expression and activation of the pro-survival Bcl-2 over the pro-apoptotic BID, and thus to pave the way for survival of the apoptotic neuron subjected to chronic ER stress.** On d 6 of the differentiation period, post-mitotic neurones from the LUHMES cell line were treated with 0 and 100 nM of thapsigargin (TG) in the presence or absence of 100 nM Liraglutide (LIRA) or of 100 nM novel GLP-1/GIP Dual Agonist (DA) for 16 h. Neurones were then harvested, and 0.3 mg mL^{-1} protein of whole-cell lysate was processed with the PathScan® sandwich immunoassay. All protein samples per experiment were processed in duplicate. Each bar represents the mean ± SEM from five independent experiments. Data are expressed as fold change to the control (CNTRL; unstressed/untreated conditions) and analysed by two-way ANOVA, followed by *post hoc* Bonferroni's multiple comparison t-test: $^{*}p \leq 0.05$, $^{**}p \leq 0.01$ & $^{***}p \leq 0.001$ compared to CNTRL; $^{\sharp}p \leq 0.05$, $^{\sharp\sharp}p \leq 0.01$, $^{\sharp\sharp\sharp}p \leq 0.001$, & $^{ns}p \gg 0.05$ compared to the TG-treated neurones.

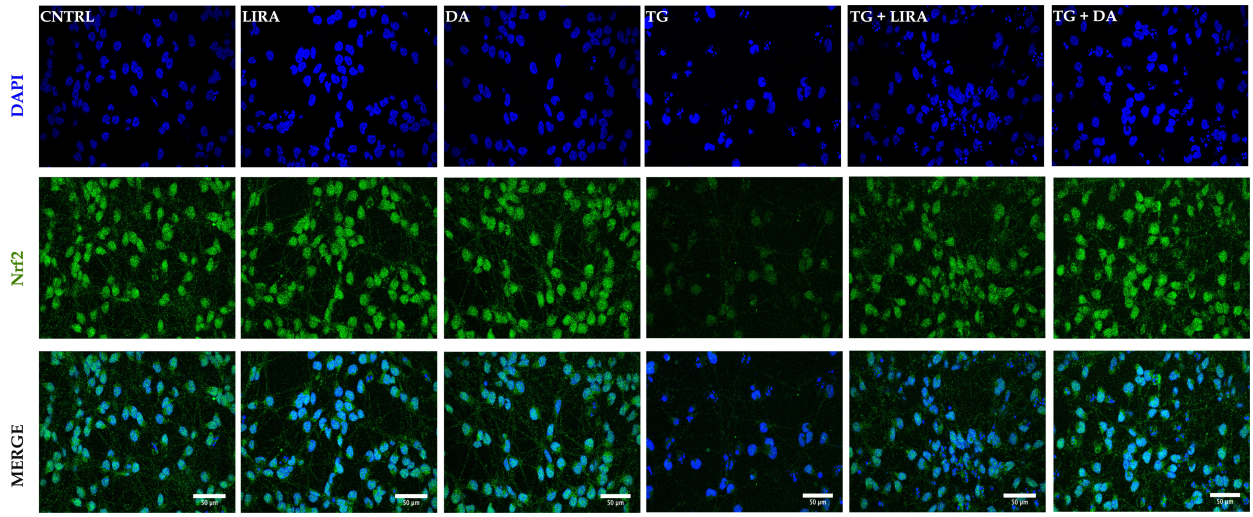
CNTRL
LIRA
DA
TG
TG + LIRA
TG + DA
DAPI
Nrf2
MERGE

(a)

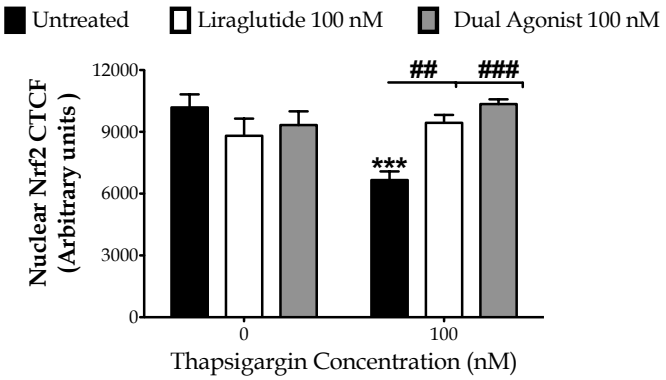
Untreated
Liraglutide 100 nM
Dual Agonist 100 nM
Nuclear Nrf2 CTCF (Arbitrary units)
12000
9000
6000
3000
0
##
###
***
0
100
Thapsigargin Concentration (nM)

(b)

Figure 9: **Liraglutide (LIRA) and the GLP-1/GIP dual agonist (DA) reinstates homeostasis of the attenuated signalling of the nuclear factor erythroid 2-related factor 2 (Nrf2) upon irremediable neuronal ER stress.** On d 6 of the differentiation period, post-mitotic neurones from the LUHMES cell line were treated with 0 and 100 nM of thapsigargin (TG) in the presence or absence of each incretin tested for 16 h. All cell treatments were performed in duplicate per experiment. Neurones were (para-formaldehyde)-fixed, immunolabelled for Nrf2 and processed for confocal imaging at 40X magnification, as shown in the representative images [**(a)**]. Six pictures were captured per treatment sample per experiment for quantification. Image J was used to quantify corrected total cell fluorescence (CTCF) of the nuclear Nrf2 staining [**(b)**]. Each bar represents the mean ± SEM from five independent experiments. Data processed with two-way ANOVA, followed by *post hoc* Bonferroni's multiple comparison t-test: $^{***}p \leq 0.001$ compared to CNTRL; $^{\sharp\sharp}p \leq 0.01$ & $^{\sharp\sharp\sharp}p \leq 0.001$ compared to the TG-stressed neurones. Scale bars: 50 µm.